First, we examined the role of ASPP2 in TJ formation. Depolarized control or *ASPP2*-RNAi cells were supplied with calcium (calcium switch, CS) to make cell-cell contacts, and TJ formation was monitored by staining of the TJ proteins ZO-1 and occludin. Although the formation of TJs was accomplished within 6 hr in control cells, *ASPP2*-RNAi cells exhibited a profound delay (Figure 2A). Twenty-four hours after CS, however, there were no apparent differences between control and *ASPP2*-RNAi cells. These properties of *ASPP2*-RNAi cells are very similar to those of *PAR-3*-RNAi cells [23] and suggest the involvement of ASPP2 in the formation of TJs. This notion was further confirmed by a functional measure of TJ integrity, transepithelial electrical resistance (TER) (Figure 2B) [25]. In control cells subjected to CS, the TER rose to a peak 6–8 hr after CS as the junctions matured, followed by a gradual decline. Such development of the TER was significantly abolished in *PAR-3*-RNAi cells, as reported previously [23], and in *ASPP2*-RNAi cells to a lesser extent. Taken together, these results indicate that ASPP2 is involved in the formation of TJs.

ASPP2 Is Involved in the Development and Maintenance of Apical Domains

We next examined whether ASPP2 plays a role in the development of apical membrane domains, as has been reported for PAR-3 [24]. The formation of apical domains can be monitored by the disappearance of the vacuolar apical compartments (VACs) after CS. VACs represent endocytosed apical membrane proteins that become apparent during depolarization by calcium depletion and are exocytosed to reform apical domains after CS [26]. In control MDCK cells, gp135-positive VACs induced by prolonged calcium depletion were observed in 37% (319 of 859) of cells. CS quickly resulted in the relocalization of gp135 from VACs to apical domains within 3 hr, resulting in 9.5% (115 of 1205) of cells retaining VACs (Figures 3A and 3B), as reported previously [24]. In *ASPP2*-RNAi cells, calcium depletion induced VACs at a similar level (40.9%, 409 of 1000 cells) to that of the control cells. However, the relocalization of gp135 from VACs to apical domains after CS was substantially delayed, with 24.3% (344 of 1418) of cells still containing VACs after 3 hr (Figures 3A and 3B). These effects of *ASPP2*-RNAi were further confirmed by transient transfection with two independent small interfering RNAs (siRNAs) (Figures S4A and S4B). These results indicate that ASPP2 is required for the development of apical domains.

Another measure of epithelial cell polarity mediated by the PAR complex is the recruitment of apical proteins to the cell surface from the intracellular compartment during the maintenance phase of cell polarity [22]. This phenomenon was clearly demonstrated in MDCK cells in the absence of cell-cell contact induced by low calcium conditions. Many control cells retained apical proteins such as gp135 at the cell periphery (nonsilencing, NS; Figure 3C). This apical domain retention was significantly affected in *PAR-3*-RNAi cells [22] (Figure 3D). Similarly, but to a lesser extent, *ASPP2*-RNAi cells failed to retain apical domain proteins; gp135, ezrin, and F-actin failed to distribute to the cell periphery and instead accumulated in the intracellular regions (Figure 3C). The proportion of cells retaining gp135 at the cell periphery was significantly lower in *ASPP2*-RNAi cells (28% ± 6%, n = 3) than in control cells (67% ± 2%, n = 3) (Figure 3D). Consistent results were obtained by transient transfection with two independent siRNAs against *ASPP2* (Figure S4C). These data indicate that ASPP2 is required for the maintenance of apical domains.

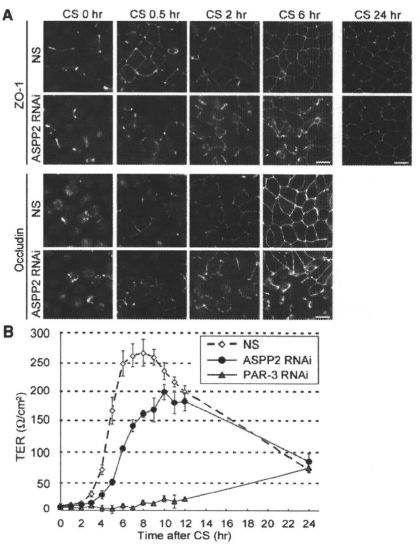

Figure 2. ASPP2 Is Required for the Efficient Formation of Tight Junctions

(A) The time course of tight junction (TJ) formation after calcium switch (CS) was compared between NS and *ASPP2*-RNAi MDCK cells by immunostaining for ZO-1 or occludin. Confluent MDCK cells cultured on permeable filters were subjected to low calcium medium for 20 hr and observed at each time point (0 to 24 hr) after the restoration of calcium, as indicated. Scale bars represent 10 μm.

(B) The development of transepithelial electrical resistance (TER) was compared between NS, *ASPP2*-RNAi, and *PAR-3*-RNAi MDCK cells by measuring it at different times after CS. The error bars indicate the standard deviation (SD; n = 3).

ASPP2 Colocalizes with PAR-3 to Primordial Cell-Cell Contacts

Physical interaction and an intimate functional relationship between ASPP2 and PAR-3 suggest the importance of the colocalization of ASPP2 and PAR-3 in the regulation of epithelial cell polarity. We compared the distribution of ASPP2 and PAR-3 during the polarization process. In polarized MDCK cells, ASPP2 and the components of the PAR complex localize to the apical junctions (Figures 1C and 1E) [20, 27]. On the other hand, they move to different compartments in depolarized cells: aPKC and PAR-6β move to VACs, whereas PAR-3 remains at the cell periphery (Figure 3F), although the exact destination of PAR-3 has not been established [24]. Importantly, ASPP2 was not detected in VACs, but it distributed to the cell periphery and to the remaining cell-cell contacts with ZO-1 (Figures 3E and 3F), showing a sharp contrast to aPKC and PAR-6. Note that nonspecific signals were possibly observed following nuclear staining of ASPP2 under low calcium conditions, because only the signals in cell-cell junctions were diminished by RNAi against *ASPP2* (Figure S3B). Furthermore, ASPP2 and PAR-3 colocalized to the fragmentally remaining cell-cell contacts labeled with ZO-1 in low

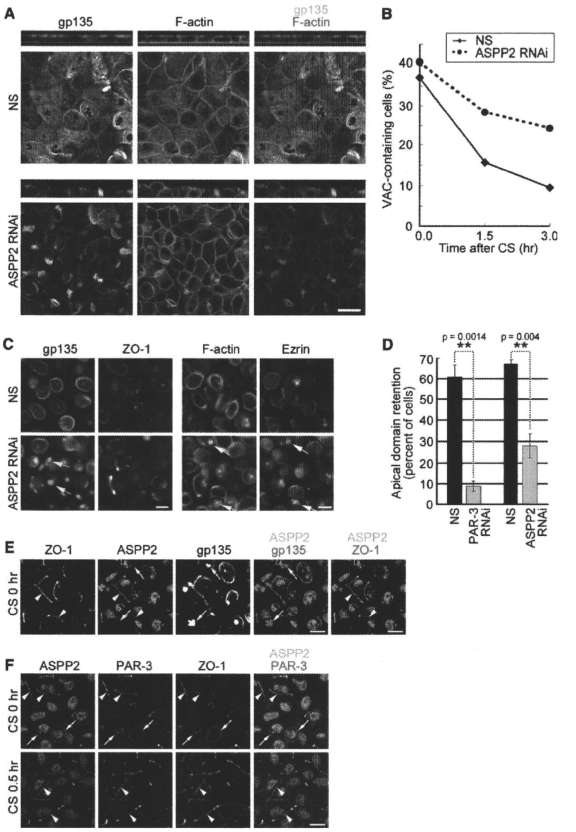

Figure 3. ASPP2 Is Required for the Development and Maintenance of Apical Domains in MDCK Cells

(A) The development of apical domains was assessed 3 hr after CS in NS and *ASPP2*-RNAi MDCK cells. The apical domains were labeled with gp135, and the whole cell cortices, including the vacuolar apical compartments (VACs), were labeled for F-actin. Projected views of confocal sections are presented with z sectional views. *ASPP2*-RNAi cells contain large intracellular aggregates positive for gp135 and F-actin, representing VACs, which indicate failure of appropriate apical domain development.

(B) The time courses of VAC exocytosis induced by CS (time 0) were quantified for NS control (diamonds) and *ASPP2*-RNAi (circles) MDCK cells.

(C) Confluent monolayers of NS and *ASPP2*-RNAi MDCK cells on permeable filters were subjected to low calcium medium for more than 20 hr. The retention of apical domains was analyzed by labeling for gp135, F-actin, or ezrin, whereas the disassembled cell-cell junctions were confirmed by labeling for ZO-1 or F-actin. The representatives from three independent experiments are shown, and each photograph represents the projected views of confocal sections from the apical to the basal membrane of cells. Arrows indicate VACs.

(D) Quantification of the cells retaining apical domains with peripheral gp135 staining, as indicated in (C). *PAR-3*-RNAi cells served as a positive control for the experimental procedures. The percentage of the total cells (at least 460 cells) is shown as the mean value (±SD) of three independent experiments. The p values were determined by two-tailed Student's t test.

(E) Confluent MDCK cells cultured on a permeable filter were subjected to a low calcium medium for 20 hr. VACs are identified as large intracellular structures strongly stained for gp135, a representative marker for apical domains (arrows). ASPP2 colocalizes with ZO-1 at the remaining cell-cell contacts (arrowheads).

(F) MDCK cells cultured for more than 20 hr in low calcium conditions were restored with 1.8 mM Ca^{2+} for 30 min (CS 0.5 hr). The localization of ASPP2 (green), PAR-3 (magenta), and ZO-1 is demonstrated in projected views of optical sections from the apical to the basal membranes of cells. Proteins distributed at the cell periphery and cell-cell contacts are indicated by arrows and arrowheads, respectively.

Scale bars represent 10 μm (A, C, E, and F).

calcium conditions and to the primordial cell-cell contacts during epithelial polarization shortly after restoring calcium (Figure 3F). These observations strongly support the occurrence of the ASPP2-PAR-3 complex at primordial cell-cell contacts before aPKC-PAR-6β is recruited to PAR-3 [24, 28].

ASPP2 Forms a Protein Complex with PAR-3 Independently of Lgl

The activity of the PAR-3-aPKC-PAR-6 complex is negatively regulated by Lgl, which competes for the aPKC-PAR-6 complex with PAR-3 [22]. To evaluate the involvement of ASPP2 in this process, we examined whether Lgl-1/2 affected the interaction between ASPP2 and PAR-3. Depletion of Lgl-1/2 clearly increased the amounts of aPKC and PAR-6β coprecipitated with PAR-3, confirming the enhanced association of the aPKC-PAR6β complex with PAR-3 (Figure 4A) [22]. However, depletion of Lgl-1/2 did not significantly affect the amount of ASPP2 coprecipitated with PAR-3. Consistently, depletion of Lgl-1/2 did not significantly increase the amount of PAR-3 coprecipitated with ASPP2, whereas the levels of aPKC and PAR-6β were increased. These results suggest that the interaction between ASPP2 and PAR-3 is independent of Lgl. Taken together with the colocalization of ASPP2 and PAR-3 from the initial phase of polarization, our observations support the intimate relationship between these proteins.

The Interaction between ASPP2 and PAR-3 Is Required for Epithelial Cell Polarity

The close functional relationship and colocalization of ASPP2 and PAR-3 allowed us to examine the mutual relationship between ASPP2 and PAR-3 in terms of their localization. We found that the signals for ASPP2 in cell-cell junctions were

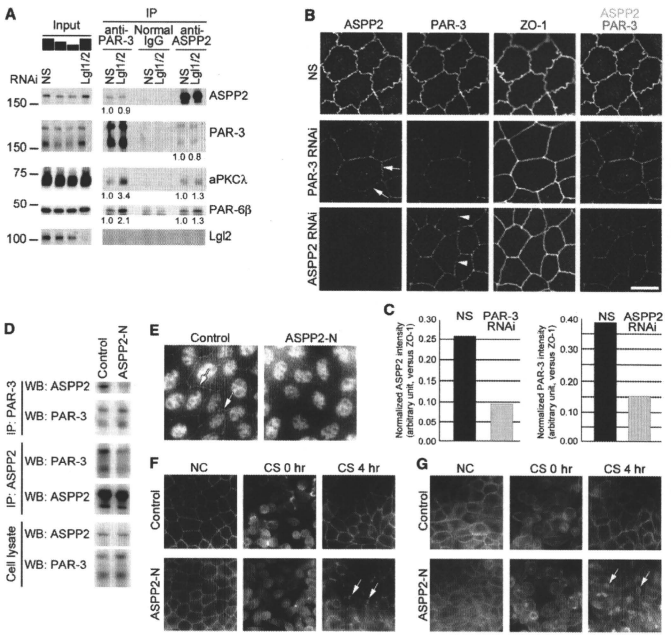

Figure 4. Interaction between ASPP2 and PAR-3 Is Required for Epithelial Cell Polarity

(A) NS and *Lgl-1/2* double RNAi MDCK cells were subjected to immunoprecipitation with the indicated antibodies. Fractions of the cell lysate (input: NS, 0.3%, 0.2%, and 0.15%; *Lgl-1/2*-RNAi, 0.3%) and coprecipitated proteins (IP, 20% each) were analyzed by western blotting using antibodies against the indicated proteins. Relative intensities are shown in numbers below the bands.

(B) ASPP2 (green), PAR-3 (magenta), and ZO-1 were localized in confluent monolayers of NS, *PAR-3*-RNAi, and *ASPP2*-RNAi MDCK cells. Single confocal sections at the apical side demonstrate substantially diminished signals for ASPP2 (arrows) or PAR-3 (arrowheads) in the cell-cell junctions in *PAR-3*- or *ASPP2*-RNAi cells, respectively. Instead, the signals for ZO-1 were not notably altered. Scale bar represents 10 μm.

(C) Quantification of the normalized signals for ASPP2 (top) or PAR-3 (bottom) in *PAR-3*- or *ASPP2*-RNAi cells, respectively. The signals were normalized against ZO-1 staining, and the means of two independent experiments are shown.

(D) MDCK cells expressing or not expressing the N-terminal part of ASPP2 (ASPP2-N) were subjected to immunoprecipitation with the indicated antibodies. Fractions of the cell lysate and coprecipitated proteins were analyzed by western blotting using the indicated antibodies.

(E) The localization of endogenous ASPP2 was analyzed in control and ASPP2-N-expressing MDCK cells. The signals for ASPP2 were substantially reduced in ASPP2-N-expressing MDCK cells (arrows).

(F and G) The formation of TJs and apical domains after CS was compared between control and ASPP2-N-expressing MDCK cells by labeling for ZO-1 (F) or F-actin (G). Arrows indicate incomplete formation of TJs (F) or remaining VACs (G).

substantially diminished in *PAR-3*-RNAi cells, although RNAi against either *ASPP2* or *PAR-3* did not apparently affect the signals for ZO-1 in confluent MDCK cells (Figures 4B and 4C). Similarly, the signals for PAR-3 were significantly reduced in *ASPP2*-RNAi cells. Note that the expression level of ASPP2 was not affected in *PAR-3*-RNAi cells, and vice versa, in either normal or low calcium conditions (Figure 1D). These results indicate the mutual dependence of ASPP2 and PAR-3 for their localization at apical cell-cell junctions, further supporting the close functional relationship between ASPP2 and the PAR complex.

To investigate the physiological significance of the interaction between ASPP2 and PAR-3, we utilized overexpression of the N-terminal part of ASPP2 (ASPP2-N; Figure S2E) to perturb this interaction. Immunoprecipitation analysis of MDCK cells expressing ASPP2-N revealed interference in the formation of the complex between endogenous ASPP2 and PAR-3 (Figure 4D). These cells demonstrated reduced localization of endogenous ASPP2 at cell-cell junctions, suggesting that the localization is dependent on the interaction with PAR-3 (Figure 4E). Importantly, these cells also showed delayed formation of cell-cell junctions and apical domains after CS (Figures 4F and 4G). These data demonstrate that the interaction between ASPP2 and PAR-3 is important in the regulation of epithelial cell polarity.

Conclusions

In this study, we provide evidence that ASPP2 plays critical roles in the establishment and maintenance of epithelial

apical-basal polarity by mediating the PAR complex formation through the regulation of PAR-3 localization. In addition to epithelial polarity, the PAR complex has been shown to regulate asymmetric cell division [1, 13, 14]. Furthermore, a recent report has shown that p53 regulates the polarity of self-renewing division of mammary stem cells [29]. However, the molecular mechanisms have not yet been elucidated. Considering the role of ASPP as an important mediator of p53 [10, 12], our data may shed light on a possible link between cell fate determination by p53 and the regulation of cell polarity by the ASPP2-PAR-3 complex.

Experimental Procedures

Cell Culture

MDCK II cells were grown in Dulbecco's modified Eagle's medium (DMEM; Nissui Pharmaceutical) containing 10% fetal calf serum (FCS), penicillin, and streptomycin (BioWhittaker) at 37°C in a 5% CO_2 atmosphere at constant humidity. For the Ca^{2+}-depletion assay, cells were seeded on Transwell filters (12 mm diameter, 0.4 μm pore size; Corning Coaster) at 2×10^5 cells/cm^2 and grown for 1 or 2 days to produce a confluent monolayer. Cells were washed twice with phosphate-buffered saline and incubated in a low Ca^{2+} (LC) medium containing 5% FCS, 3 μM Ca^{2+}, penicillin, and streptomycin for more than 20 hr. The Ca^{2+} switch assay was performed by replacing the LC medium restored with 1.8 mM Ca^{2+}.

Expression Vectors

For generating MDCK cells stably expressing SBP-tagged proteins under the control of tetracycline-inducible transactivation, the SacI-PvuI fragment of the pNTAP vector (Stratagene) was first cloned into the EcoRV and PstI sites of the pOS-Tet14MCS vector (a generous gift from Y. Miwa, Tsukuba University) after blunting, and then a cDNA encoding rat PAR-3 (1–1333 aa) [27] or mouse sPAR-3 (1–1034 aa) [21] was cloned into the EcoRV site. cDNAs encoding rat PAR-3 (1–1333 aa) and human ASPP2 (2–1128 aa; IMAGE cDNA clone ID 4537206, GenBank ID Q13625) were subcloned into the SR-HA and SR-V5 mammalian expression vectors, respectively.

RNAi for *ASPP2* in MDCK Cells

Nonsilencing control and *ASPP2*-RNAi MDCK clones were established by stable transfection with pSUPERIOR.neo vectors (Oligoengine) encoding a scramble sequence (5′-CAGUCGCGUUUGCGACUGG-3′; Dharmacon Research) [22, 30] and the canine *ASPP2* siRNA sequence (*ASPP2*-siRNA1, #2315: 5′-GCACUUCUCCACUGUUUAUGG-3′), respectively. The *PAR-3*-RNAi MDCK stable clone was described previously [22]. The sequences of siRNAs used were nonsilencing control (QIAGEN Cat# 1027281), *ASPP2*-siRNA1 (#2315), and *ASPP2*-siRNA2 (#3326: 5′-GUUCCUCGUGCAAUUUG GUGU-3′). The *ASPP2* siRNAs were designed to avoid any off-target effects on ASPP1 or iASPP.

Immunoprecipitation and Western Blot Analysis

MDCK II and 293T cells were lysed in lysis buffer containing 50 mM Tris-HCl at pH 7.5, 150 mM NaCl, 10% glycerol, 1% NP-40, 5 mM $MgCl_2$, 1 mM EGTA, 1 mM dithiothreitol, protease inhibitor cocktail (SIGMA), and phosphatase inhibitor cocktail (Roche). After centrifugation at 20,000 × g for 30 min, the supernatants were subjected to immunoprecipitation with the indicated antibodies followed by SDS-PAGE and western blotting, as described previously [22].

Antibodies

The rabbit anti-ASPP2 antibodies, C2AP and C3AP, were raised against aa 773–912 of human ASPP2 fused with glutathione-*S*-transferase and were affinity purified (Scrum). Rat anti-PAR-3 polyclonal antibody (pAb) (CR1-2AP) and rabbit anti-PAR-6β pAb (BC31AP) were described previously [20, 24]. Antibodies purchased were rabbit anti-PAR-3 pAb (07-330; Upstate), mouse anti-aPKCι monoclonal antibody (mAb; clone 23; BD Transduction Laboratories), mouse anti-occludin mAb (clone OC-3F10; Zymed), mouse anti-E-cadherin mAb (clone 36; BD Transduction Laboratories), rabbit anti-aPKCζ/λ pAb (SC-216; Santa Cruz Biotechnology), rat anti-ZO-1 mAb (clone R40.76; Santa Cruz Biotechnology), rabbit anti-14-3-3β pAb (SC-629; Santa Cruz Biotechnology), mouse anti-ezrin mAb (clone 3C12; Sigma), and mouse anti-Lgl2 mAb (clone 4G2; Abnova). Mouse anti-gp135 mAb (clone 3F2/D8) was a gift from George K. Ojakian (State University of New York).

Immunofluorescence Microscopy

MDCK cells were fixed with 2% paraformaldehyde (PFA) and stained as described previously [31]. The primary antibodies were visualized using Alexa Fluor 488-, 555-, or 647-conjugated secondary antibodies (Molecular Probes). Rhodamine-phalloidin was used to visualize filamentous actin (Molecular Probes). Samples were mounted with ProLong Gold (Invitrogen) and were observed using a confocal microscope system (LSM 510; Carl Zeiss) or a fluorescence microscope (BX50; Olympus) equipped with a cooled charge-coupled device camera (Sensys 1400G2; Photometrics). Acquired images were analyzed using Photoshop (Adobe Systems), Multi Gauge (Fujifilm), or ImageJ (National Institutes of Health), according to the guidelines of the journal.

Mouse (ICR; Japan CLEA) kidneys and duodenum were perfused and immersed in 0.1 M HEPES-NaOH buffer (pH 7.4) containing 4% PFA, 2.5 mM $CaCl_2$, 1.25 mM $MgCl_2$, and 2.9% glucose for 2 hr at room temperature [32] and were processed for cryosectioning. The cryosections were processed for heat-induced epitope retrieval by incubating in a target retrieval solution (S1700; DAKO) for 15 min at 121°C, and they were labeled with anti-ASPP2 antibody (2.5 μg/ml, 16.7 nM) with 3.0 nM of the corresponding antigen or GST. All animal experiments were conducted in accordance with the Guidelines for Proper Conduct of Animal Experiments (Science Council of Japan), and all protocols were approved by our institutional review boards.

Supplemental Information

Supplemental Information includes four figures and can be found with this article online at doi:10.1016/j.cub.2010.06.024.

Acknowledgments

We are grateful to Y. Miwa and G.K. Ojakian for reagents, all the members of the Ohno laboratory for helpful discussions, and Rie Kurata and Chiho Kusaka for their technical assistance. This work was supported by the Yokohama City University Center of Excellence Program of the Ministry of Education, Culture, Sports, Science and Technology of Japan (MEXT) (S.O.). This work was also supported in part by grants from the Japan Society for the Promotion of Science and from MEXT (T.H., Y.H., A.Y., K.M., H.H., and S.O.) and by a grant from the 2009 Strategic Research Project of Yokohama City University (T.H.).

Received: December 4, 2009
Revised: May 21, 2010
Accepted: June 10, 2010
Published online: July 8, 2010

References

1. Kemphues, K. (2000). PARsing embryonic polarity. Cell *101*, 345–348.
2. Ohno, S. (2001). Intercellular junctions and cellular polarity: The PAR-aPKC complex, a conserved core cassette playing fundamental roles in cell polarity. Curr. Opin. Cell Biol. *13*, 641–648.
3. Suzuki, A., and Ohno, S. (2006). The PAR-aPKC system: Lessons in polarity. J. Cell Sci. *119*, 979–987.
4. Goldstein, B., and Macara, I.G. (2007). The PAR proteins: Fundamental players in animal cell polarization. Dev. Cell *13*, 609–622.
5. Hirose, T., Karasawa, M., Sugitani, Y., Fujisawa, M., Akimoto, K., Ohno, S., and Noda, T. (2006). PAR3 is essential for cyst-mediated epicardial development by establishing apical cortical domains. Development *133*, 1389–1398.
6. Imai, F., Hirai, S., Akimoto, K., Koyama, H., Miyata, T., Ogawa, M., Noguchi, S., Sasaoka, T., Noda, T., and Ohno, S. (2006). Inactivation of aPKClambda results in the loss of adherens junctions in neuroepithelial cells without affecting neurogenesis in mouse neocortex. Development *133*, 1735–1744.
7. Costa, M.R., Wen, G., Lepier, A., Schroeder, T., and Götz, M. (2008). Par-complex proteins promote proliferative progenitor divisions in the developing mouse cerebral cortex. Development *135*, 11–22.
8. Hirose, T., Satoh, D., Kurihara, H., Kusaka, C., Hirose, H., Akimoto, K., Matsusaka, T., Ichikawa, I., Noda, T., and Ohno, S. (2009). An essential

role of the universal polarity protein, aPKClambda, on the maintenance of podocyte slit diaphragms. PLoS ONE *4*, e4194.

9. Bultje, R.S., Castaneda-Castellanos, D.R., Jan, L.Y., Jan, Y.N., Kriegstein, A.R., and Shi, S.H. (2009). Mammalian Par3 regulates progenitor cell asymmetric division via notch signaling in the developing neocortex. Neuron *63*, 189–202.
10. Trigiante, G., and Lu, X. (2006). ASPP [corrected] and cancer. Nat. Rev. Cancer *6*, 217–226.
11. Vives, V., Su, J., Zhong, S., Ratnayaka, I., Slee, E., Goldin, R., and Lu, X. (2006). ASPP2 is a haploinsufficient tumor suppressor that cooperates with p53 to suppress tumor growth. Genes Dev. *20*, 1262–1267.
12. Sullivan, A., and Lu, X. (2007). ASPP: A new family of oncogenes and tumour suppressor genes. Br. J. Cancer *96*, 196–200.
13. Knoblich, J.A. (2008). Mechanisms of asymmetric stem cell division. Cell *132*, 583–597.
14. Morrison, S.J., and Kimble, J. (2006). Asymmetric and symmetric stem-cell divisions in development and cancer. Nature *441*, 1068–1074.
15. Kalluri, R., and Weinberg, R.A. (2009). The basics of epithelial-mesenchymal transition. J. Clin. Invest. *119*, 1420–1428.
16. Bryant, D.M., and Mostov, K.E. (2008). From cells to organs: Building polarized tissue. Nat. Rev. Mol. Cell Biol. *9*, 887–901.
17. Wang, Q., and Margolis, B. (2007). Apical junctional complexes and cell polarity. Kidney Int. *72*, 1448–1458.
18. Etienne-Manneville, S. (2004). Cdc42—the centre of polarity. J. Cell Sci. *117*, 1291–1300.
19. Iden, S., and Collard, J.G. (2008). Crosstalk between small GTPases and polarity proteins in cell polarization. Nat. Rev. Mol. Cell Biol. *9*, 846–859.
20. Yamanaka, T., Horikoshi, Y., Sugiyama, Y., Ishiyama, C., Suzuki, A., Hirose, T., Iwamatsu, A., Shinohara, A., and Ohno, S. (2003). Mammalian Lgl forms a protein complex with PAR-6 and aPKC independently of PAR-3 to regulate epithelial cell polarity. Curr. Biol. *13*, 734–743.
21. Mizuno, K., Suzuki, A., Hirose, T., Kitamura, K., Kutsuzawa, K., Futaki, M., Amano, Y., and Ohno, S. (2003). Self-association of PAR-3-mediated by the conserved N-terminal domain contributes to the development of epithelial tight junctions. J. Biol. Chem. *278*, 31240–31250.
22. Yamanaka, T., Horikoshi, Y., Izumi, N., Suzuki, A., Mizuno, K., and Ohno, S. (2006). Lgl mediates apical domain disassembly by suppressing the PAR-3-aPKC-PAR-6 complex to orient apical membrane polarity. J. Cell Sci. *119*, 2107–2118.
23. Chen, X., and Macara, I.G. (2005). Par-3 controls tight junction assembly through the Rac exchange factor Tiam1. Nat. Cell Biol. *7*, 262–269.
24. Horikoshi, Y., Suzuki, A., Yamanaka, T., Sasaki, K., Mizuno, K., Sawada, H., Yonemura, S., and Ohno, S. (2009). Interaction between PAR-3 and the aPKC-PAR-6 complex is indispensable for apical domain development of epithelial cells. J. Cell Sci. *122*, 1595–1606.
25. Madara, J.L., and Dharmsathaphorn, K. (1985). Occluding junction structure-function relationships in a cultured epithelial monolayer. J. Cell Biol. *101*, 2124–2133.
26. Vega-Salas, D.E., Salas, P.J., and Rodriguez-Boulan, E. (1988). Exocytosis of vacuolar apical compartment (VAC): A cell-cell contact controlled mechanism for the establishment of the apical plasma membrane domain in epithelial cells. J. Cell Biol. *107*, 1717–1728.
27. Izumi, Y., Hirose, T., Tamai, Y., Hirai, S., Nagashima, Y., Fujimoto, T., Tabuse, Y., Kemphues, K.J., and Ohno, S. (1998). An atypical PKC directly associates and colocalizes at the epithelial tight junction with ASIP, a mammalian homologue of Caenorhabditis elegans polarity protein PAR-3. J. Cell Biol. *143*, 95–106.
28. Suzuki, A., Ishiyama, C., Hashiba, K., Shimizu, M., Ebnet, K., and Ohno, S. (2002). aPKC kinase activity is required for the asymmetric differentiation of the premature junctional complex during epithelial cell polarization. J. Cell Sci. *115*, 3565–3573.
29. Cicalese, A., Bonizzi, G., Pasi, C.E., Faretta, M., Ronzoni, S., Giulini, B., Brisken, C., Minucci, S., Di Fiore, P.P., and Pelicci, P.G. (2009). The tumor suppressor p53 regulates polarity of self-renewing divisions in mammary stem cells. Cell *138*, 1083–1095.
30. Suzuki, A., Hirata, M., Kamimura, K., Maniwa, R., Yamanaka, T., Mizuno, K., Kishikawa, M., Hirose, H., Amano, Y., Izumi, N., et al. (2004). aPKC acts upstream of PAR-1b in both the establishment and maintenance of mammalian epithelial polarity. Curr. Biol. *14*, 1425–1435.
31. Hirose, T., Izumi, Y., Nagashima, Y., Tamai-Nagai, Y., Kurihara, H., Sakai, T., Suzuki, Y., Yamanaka, T., Suzuki, A., Mizuno, K., and Ohno, S. (2002). Involvement of ASIP/PAR-3 in the promotion of epithelial tight junction formation. J. Cell Sci. *115*, 2485–2495.
32. Yamashita, S., Katsumata, O., and Okada, Y. (2009). Establishment of a standardized post-embedding method for immunoelectron microscopy by applying heat-induced antigen retrieval. J. Electron Microsc. (Tokyo) *58*, 267–279.

THE JOURNAL OF BIOLOGICAL CHEMISTRY VOL. 285, NO. 46, pp. 35311–35319, November 12, 2010

Contribution of Lysine 11-linked Ubiquitination to MIR2-mediated Major Histocompatibility Complex Class I Internalization*[S]

Received for publication, February 9, 2010, and in revised form, September 9, 2010 Published, JBC Papers in Press, September 10, 2010, DOI 10.1074/jbc.M110.112763

Eiji Goto[‡], Yuko Yamanaka[§], Akiyo Ishikawa[§], Masami Aoki-Kawasumi[‡], Mari Mito-Yoshida[‡], Mari Ohmura-Hoshino[‡], Yohei Matsuki[‡§], Mizuho Kajikawa[‡], Hisashi Hirano[§], and Satoshi Ishido[‡§1]

From the [‡]Laboratory for Infectious Immunity, RIKEN Research Center for Allergy and Immunology, 1-7-22 Suehiro-cho, Tsurumi-ku, Yokohama, Kanagawa 230-0045 and [§]Supramolecular Biology, International Graduate School of Arts and Sciences, Yokohama City University, 1-7-29 Suehiro-cho, Tsurumi-ku, Yokohama, Kanagawa 230-0045, Japan

The polyubiquitin chain is generated by the sequential addition of ubiquitin moieties to target molecules, a reaction between specific lysine residues that is catalyzed by E3 ubiquitin ligase. The Lys[48]-linked and Lys[63]-linked polyubiquitin chains are well established inducers of proteasome-dependent degradation and signal transduction, respectively. The concept has recently emerged that polyubiquitin chain-mediated regulation is even more complex because various types of atypical polyubiquitin chains have been discovered *in vivo*. Here, we demonstrate that a novel complex ubiquitin chain functions as an internalization signal for major histocompatibility complex class I (MHC I) membrane proteins *in vivo*. Using a tetracycline-inducible expression system and quantitative mass spectrometry, we show that the polyubiquitin chain generated by the viral E3 ubiquitin ligase of Kaposi sarcoma-associated herpesvirus, MIR2, is a Lys[11] and Lys[63] mixed-linkage chain. This novel ubiquitin chain can function as an internalization signal for MHC I through its association with epsin1, an adaptor molecule containing ubiquitin-interacting motifs.

The functions of many membrane proteins, including various signal-transducing receptors, are regulated by internalization, following which the receptors are either recycled or degraded in lysosomes (1). Dysregulation of this process is thought to underlie many disorders, including cancer and autoimmunity (2–5); consequently, it is important to gain an understanding of the molecular mechanisms of receptor internalization *in vivo*. In this context, polyubiquitination is an important signal for the internalization of mammalian membrane proteins (6–10). However, it is still unclear how the presence of a polyubiquitin chain regulates the internalization step because it has been reported that monoubiquitination is sufficient to induce protein internalization in yeast (11, 12).

Monoubiquitination creates an isopeptide bond between a lysine of the target protein and the C-terminal glycine of ubiquitin. Polyubiquitination then results from the sequential linkage of additional ubiquitin moieties via specific lysine residues on ubiquitin, a process catalyzed by E3 ubiquitin ligase (E3) (13). All seven lysine residues (Lys[6], Lys[11], Lys[27], Lys[29], Lys[33], Lys[48], and Lys[63]) on ubiquitin can be utilized for the formation of polyubiquitin chains (14). Among them, Lys[48] and Lys[63] have been classically reported as the acceptor lysine residues for the generation of the polyubiquitin chain. The Lys[48]-linked and Lys[63]-linked polyubiquitin chains are well established inducers of proteasome-dependent degradation and signal transduction, respectively (15). Recently, it has been reported that lysine residues other than Lys[48] and Lys[63] can be utilized for chain formation (14). For example, Lys[29]-linked polyubiquitination of Deltex by Itch/AIP4 and Lys[27]-linked polyubiquitination of Jun were reported to be important for their lysosomal degradation (16, 17). In addition, Lys[11]-linked polyubiquitin chains were reported to be involved in cell cycle control by the anaphase-promoting complex and in endoplasmic reticulum-associated degradation of misfolded proteins (18, 19).

Among the several types of polyubiquitin chains, the Lys[63]-linked chain has been reported as an inducer of protein internalization (6, 8, 10). Recent structural analysis has demonstrated that the adaptor protein epsin1 recognizes Lys[63]-linked chains through its ubiquitin-interacting motif (UIM)[2] (20). Epsin1 contains several other conserved domains in addition to the UIM: an epsin N-terminal homology domain involved in the interaction with phosphatidylinositol 4,5-bisphosphate (21), DPW (Asp-Pro-Trp) repeat domains that include adaptor protein complex AP-2 and clathrin binding sites, and NPF (Asn-Pro-Phe) repeat domains located in the C-terminal region (22). Because epsin1 contributes to clathrin-mediated internalization, it is thought to be involved in polyubiquitination-induced internalization *in vivo* (23, 24).

To examine how polyubiquitination regulates protein internalization, we previously generated a tetracycline-inducible (Tet-on) system for a member of the MIR family (25, 26). MIR family members are membrane-bound E3 ubiquitin ligases and have been reported to induce ubiquitination-dependent internalization *in vivo* (25, 26). Use of this Tet-on system allowed us

* This work was supported in part by a grant-in-aid for scientific research from the Ministry of Education, Culture, Sports, Science, and Technology of Japan and by the Japan Society for the Promotion of Science.

[S] The on-line version of this article (available at http://www.jbc.org) contains supplemental "Experimental Procedures" and Figs. S1–S13.

[1] To whom correspondence should be addressed: 1-7-22 Suehiro-cho, Tsurumi-ku, Yokohama, Kanagawa 230-0045, Japan. Fax: 81-45-503-7021; E-mail: ishido@rcai.riken.jp.

[2] The abbreviations used are: UIM, ubiquitin-interacting motif; Dox, doxycycline; EGFP, enhanced green fluorescent protein; MIR, modulator of immune recognition; Tet-on, tetracycline-inducible.

to visualize the detailed status of polyubiquitin chains that induce internalization *in vivo* (25). Recently, Gygi and colleagues have also successfully developed a detection system for polyubiquitin chains generated *in vivo* that uses mass spectrometry (27, 28). In the study reported here, we have combined our Tet-on expression system for MIR2 with quantitative mass spectrometry to address the issue of how the polyubiquitin chain contributes to receptor internalization. We report here that the polyubiquitin chain generated by MIR2 is a novel Lys^{11} and Lys^{63} mixed-linkage chain and that this mixed polyubiquitin chain is required for efficient epsin1-dependent internalization of major histocompatibility class I (MHC I) molecules.

EXPERIMENTAL PROCEDURES

Materials—Mutants were constructed by overlapping PCR as described previously (25). Each cDNA was subcloned into the p3×FLAG-CMV (Sigma), pcDNA3 (Invitrogen), or pEGFP-N1 (Clontech) vectors. The hemagglutinin-tagged ubiquitin-expressing plasmid and the enhanced green fluorescent protein (EGFP)-tagged ubiquitin-expressing plasmid were gifts from Dr. N. Tanaka and Dr. K. Umebayashi, respectively (29). We generated T-REx-MIR2 as described previously (25). Briefly, the His-Myc-tagged MIR2-expressing cassette used in our previous study (30) was transferred into the pcDNA5/FRT/TO vector. T-REx-MIR2 cells were generated using the Flp-In™ T-REx™ Core kit (Invitrogen). The T-REx-MIR2 cells were transfected with each CD8-MHC I chimera-expressing plasmid constructed in the p3×FLAG-CMV vector and selected by incubation with 2 mg/ml G418 (Sigma) for 3 weeks. The CD8 chimera-expressing population was sorted with the FACSVantage S.E. Turbo.

Internalization Assay and Antibodies—The internalization assay was performed as reported previously (25). In brief, cells were stained with anti-CD8 Ab for 30 min at 4 °C, cultured for the indicated times at 37 °C, and then stained with phycoerythrin-conjugated goat anti-mouse IgG Ab followed by flow cytometry analysis at each time point. The percentage of the CD8 chimera remaining at the cell surface was determined by dividing the values obtained at each time point by the value obtained at time zero. In the case of the expression by ubiquitin mutants, transfected cells were stained as described above, and the GFP-positive cells were analyzed as the exogenous ubiquitin-expressing population. For immunofluorescence microscopy, FITC-labeled anti-CD8 mAb was added to the medium of T-REx-MIR2 cells, and incubation was continued for 10 min at 37 °C. After washing, the cells were analyzed by immunofluorescence microscopy. The mAbs W6/32 for MHC I, RPA-T8 for CD8, and TU36 for MHC II used for FACScan analysis were obtained from BD Biosciences. M2 anti-FLAG Ab (Sigma), F7 anti-HA Ab (Santa Cruz Biotechnology), FK2 anti-ubiquitin Ab (AFFINITI Research Products), Apu3 anti-Lys^{63} Ab (Millipore), and anti-V5 Ab (Invitrogen) were used for immunoprecipitation and/or immunoblot analysis.

Detection of Ubiquitinated Surface CD8 Chimeras and Immunoprecipitation—To examine the ubiquitination status of CD8 chimeric molecules that preexist at the plasma membrane before initiation of the ubiquitination process by MIR2, surface molecules of CD8-chimera-expressing T-REx-MIR2 cells were biotinylated followed by incubation with doxycycline (Dox) as described previously (25). The cell pellet was boiled in 1% SDS-containing radioimmune precipitation assay buffer (10 mM Tris (pH 7.5), 1% Nonidet P-40, 0.1% sodium deoxycholate, 0.15 M NaCl, 1 mM EDTA (pH 8.0)) and diluted 10-fold with SDS-free radioimmune precipitation assay buffer. CD8 chimeric molecules were precipitated with M2 anti-FLAG Ab-conjugated Sepharose (Sigma) and then eluted with FLAG peptide (150 μg/ml). The eluted CD8 chimera was further purified with streptavidin-agarose (Pierce). For immunoprecipitation, cells were harvested and lysed with Nonidet P-40 buffer (0.15 M NaCl, 1% Nonidet P-40, and 50 mM HEPES buffer (pH 8.0)) containing protease inhibitors. Immunoprecipitation was performed with the indicated antibody together with 30 μl of protein A/G-agarose beads (Santa Cruz Biotechnology). A GST pulldown assay is described in the supplemental "Experimental Procedures".

Mass Spectrometric Analysis of MHC I Ubiquitination—T-REx-MIR2 cells (12×10^7) were incubated with or without Dox (1 μg/ml) for 5 h in 10% FBS-containing RPMI 1640 medium (Sigma) to induce ubiquitination of MHC I in the presence of bafilomycin A1 (2 μM). The cells were lysed with Nonidet P-40 lysis buffer containing 200 mM NaCl, protease inhibitors, and 10 mM *N*-ethylmaleimide. Ubiquitinated CD8-MHC chimeras were purified by a two step method: the first purification was performed with anti-FLAG M2 Ab-conjugated agarose, and the second with FK2-conjugated agarose. The ubiquitinated CD8-MHC I chimeras were eluted with 0.1 M glycine-HCl (pH 2.7) and concentrated by precipitation with methanol/chloroform. To ensure that each sample contained equivalent amounts of chimeric protein, 1% of the sample purified by anti-M2 agarose affinity chromatography was examined by Western blotting with HRP-conjugated M2 antibody. In the case of analysis by SDS-PAGE, specific bands obtained from 4×10^8 T-REx-MIR2 cells were visualized in the gels by staining with Coomassie Blue, and the proteins in the excised gel slices were digested with trypsin. The resulting peptides were labeled with iTRAQ114 of multiplex iTRAQ reagents (iTRAQ reagent kit; Applied Biosystems). In the case of the analysis without SDS-PAGE, purified ubiquitinated samples from Dox(+)- and Dox(−)-treated cells were directly digested with trypsin and labeled with iTRAQ115 and iTRAQ114, respectively. To quantify the amount of each peptide derived from all types of polyubiquitin chains, diglycine signature peptides corresponding to the seven ubiquitin chain linkages were synthesized and labeled with iTRAQ117 for use as internal standards (Peptide Institute, Inc.). Labeled internal standards (1 pmol or 200 fmol) were added to the digested and labeled samples and desalted with Empore™ Extraction Disk C18 Tips. Desalted samples were separated on a MALDI plate by a direct nano-LC system equipped with a nano-LC/MALDI spotting device (DiNa Map System; KYA Technologies). MALDI plates were analyzed using the ABI 4800 MALDI-TOF/TOF Proteomics Analyzer. To acquire each MS spectrum, signature-ion peaks corresponding to 114.1, 115.1, and 117.1 were obtained by using Protein Pilot software 2.0 (Applied Biosystems). The amount of peptide corresponding to each type of polyubiquitin chain was calculated based on the signals from the internal standards.

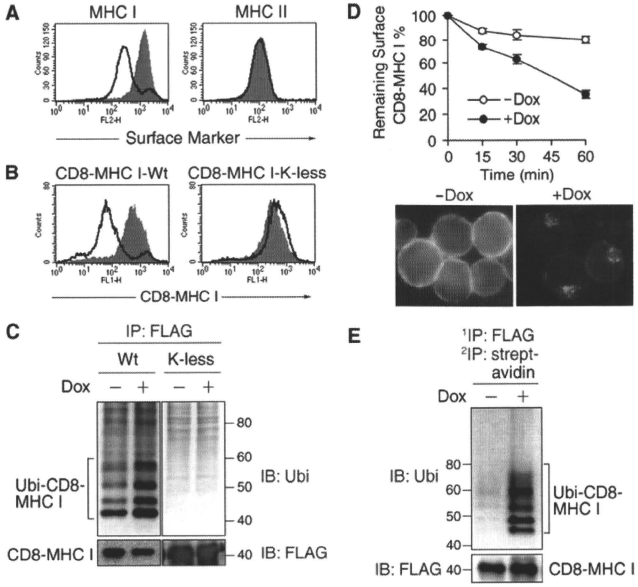

FIGURE 1. **Ubiquitination is required for MHC I down-regulation in T-REx-MIR2 cells.** *A*, after being incubated with or without Dox for 24 h, the expression level of MHC I and MHC II on T-REx-MIR2 cells was examined by flow cytometry. Data from the cells incubated with (*open histograms*) and without (*shaded histograms*) Dox are shown. *B*, the expression level of the indicated CD8 chimeras on T-REx-MIR2 cells was examined as in *A*. *C*, whole cell lysates extracted from the indicated CD8 chimera-expressing T-REx-MIR2 cells that had been cultivated with (+) or without (−) Dox for 6 h were incubated with an anti-FLAG Ab. Precipitated (*IP*) samples were probed (*IB*) with anti-FLAG M2 Ab (*FLAG*) or anti-ubiquitin FK2 Ab (*Ubi*). *D*, surface CD8-MHC I was labeled with anti-CD8 Ab after the cells were incubated with (+) or without (−) Dox for 6 h. After cultivation at 37 °C for the indicated times, the expression of the remaining surface CD8-MHC I was examined by staining with phycoerythrin-conjugated goat anti-mouse IgG. At each time point, the percentage of remaining CD8-MHC I was calculated relative to the value of labeled CD8-MHC I at 0 min (*upper panel*). In the *lower panel*, T-REx-MIR2 cells were incubated with Dox for 6 h, and FITC-conjugated anti-CD8 Ab was added for the last 10 min of culture. Internalized CD8-MHC I was observed by fluorescence microscopy. *E*, surface molecules on T-REx-MIR2 cells were biotinylated, and the cells were incubated with (+) or without (−) Dox for 6 h in the presence of 2 μM of bafilomycin A1. The biotinylated CD8-MHC I was sequentially purified with anti-FLAG Ab and streptavidin-agarose. Each sample was probed with FK2 Ab or M2 Ab.

Knockdown by RNAi—Inhibition of E2 ubiquitin-conjugating enzymes was performed by retroviral transduction of shRNAs targeting UbcH5b/c as described previously (25). For knockdown of epsin1 and clathrin heavy chain, HeLa, HeLa-MIR2, and T-REx-MIR2 cells were transfected three times at 24-h intervals with 10 pmol of siRNA/well with HiPerFect Transfection Reagent (Qiagen) and analyzed 48 h after the third transfection. Epsin1 (5′-GAACTGGCGTCACGTTTAC-3′) and clathrin heavy chain (5′-GCAATGAGCTGTTTGAAGA-3′) mRNA target sequences were purchased from Qiagen. All-Stars Negative Control siRNA was purchased as a control siRNA from Qiagen.

RESULTS

Effective Internalization of MHC Class I by Polyubiquitination in T-REx-MIR2 Cells—To examine how the polyubiquitin chain contributes to protein internalization, we used the MIR2 protein of Kaposi sarcoma-associated herpesvirus because MIR2 is known to reduce the surface expression of MHC class I (MHC I) proteins by inducing their ubiquitination-mediated internalization (31, 32). The Tet-on system for MIR2 expression, designated T-REx-MIR2, was generated as reported previously (25). To facilitate a detailed analysis of the ubiquitination and internalization of MHC I, we expressed a FLAG-tagged CD8 chimera containing the transmembrane and cytoplasmic regions of the MHC I α chain, designated CD8-MHC I, in T-REx-MIR2 cells as described previously (30). We selected these particular regions of the class I α chain for inclusion in the chimeric protein because it has been reported that CD8 chimeras containing both the transmembrane and cytoplasmic regions of MIR E3 ubiquitin ligase substrates are internalized and ubiquitinated just like the authentic endogenous substrate molecules. This seems to be the case because the transmembrane region of the substrate is thought to interact with MIRs, whereas the cytoplasmic region of the substrate contains the MIR ubiquitination site (25, 31, 32). The Dox-induced expression of MIR2 suppressed the surface expression of MHC I proteins but not of MHC class II proteins (Fig. 1*A*). As previously shown by the analysis of endogenous MHC I with MIR2 (33), the MIR2-mediated down-regulation of CD8-MHC I was mediated through the ubiquitination of cytoplasmic lysine residues; a mutant chimeric protein in which all class I cytoplasmic lysine residues were mutated to arginine was not ubiquitinated or down-regulated by MIR2 (Fig. 1, *B* and C). These results demonstrate that the CD8-MHC I chimera is a valid surrogate for native MHC I.

Next, we examined whether surface-expressed MHC I is ubiquitinated and down-regulated by MIR2. The fate of surface-expressed CD8-MHC I was examined by surface biotinylation and staining with antibody as performed in our previous studies (25). Compared with the slow turnover of surface MHC I molecules in noninduced cells, Dox-induced MIR2-expressing cells showed a much more rapid reduction (Fig. 1*D*). Concomitantly, the Dox-induced cells showed a marked increase in the ubiquitination of surface-expressed CD8-MHC I (Fig. 1*E*). To examine the relationship between ubiquitination and down-regulation of surface-expressed CD8-MHC I further, we used

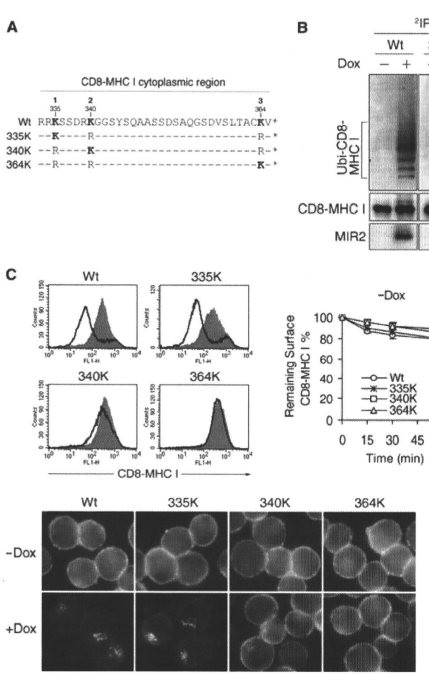

FIGURE 2. **Ubiquitination at Lys^{335} is a critical event for MHC I down-regulation by MIR2.** *A*, protein sequences of the cytoplasmic region of each CD8 mutant chimera are aligned. *B*, the indicated CD8-mutant chimera-expressing T-REx-MIR2 cells were incubated with Dox for 6 h in the presence of 2 μM bafilomycin A1, and the ubiquitination status of the chimeras was examined as in Fig. 1*E*. *C*, after being incubated with or without Dox for 9 h, the expression level of the indicated CD8 chimeras on T-REx-MIR2 cells was examined by flow cytometry. Data from the cells incubated with (*open histograms*) and without (*shaded histograms*) Dox are shown (*upper left*). In the *upper right panel*, each surface-expressed CD8 chimera was labeled with anti-CD8 Ab after the cells were incubated with (+) or without (−) Dox for 6 h. After cultivation at 37 °C for the indicated times, the expression level of the CD8 chimeric proteins remaining on the cell surface was examined as in Fig. 1*D*. At each time point, the percentage of remaining CD8 chimera was calculated relative to its level at 0 min. In the *lower panel*, the indicated CD8 mutant chimera-expressing T-REx-MIR2 cells were incubated with Dox for 6 h, and FITC-conjugated anti-CD8 Ab was added for the last 10 min of culture. The internalized CD8 chimera was observed by fluorescence microscopy.

small interfering RNA to inhibit expression of UbcH5b/c, reported to be an E2 enzyme of the MIR family of E3 ligases (25, 31). Although ubiquitination could not be completely blocked, down-regulation of surface-expressed CD8-MHC I was significantly inhibited (supplemental Fig. S1). At present, we cannot explain why incompletely blocked ubiquitination could still significantly inhibit the down-regulation of CD8-MHC I. UbcH5b/c may support the ubiquitination of other molecules that contribute to the down-regulation of CD8-MHC I. Indeed, several adaptor molecules involved in ubiquitination-mediated internalization, *e.g.* β-arrestin, have been reported to be monoubiquitinated (34). Thus, these results strongly suggest that surface-expressed CD8-MHC I is down-regulated by MIR2-mediated ubiquitination in T-REx-MIR2 cells.

We next examined the sites on MHC I that are responsible for the MIR2-mediated down-regulation. MHC I has three lysine residues (Lys^{335}, Lys^{340}, and Lys^{364}) in its cytoplasmic tail, therefore we mutated these candidate ubiquitination sites to arginine as shown in Fig. 2*A*. Each CD8-MHC I mutant was stably expressed in T-REx-MIR2 cells, and the ubiquitination status and down-regulation of the surface-expressed chimeric proteins were analyzed. Although there was some background ubiquitination of Lys^{340} and Lys^{364} in the absence of Dox, presumably due to Dox-independent MIR2 expression, Dox-induced MIR2 ubiquitinated Lys^{335} and Lys^{340} but only minimally ubiquitinated Lys^{364} (Fig. 2*B*). MHC I was only down-regulated when Lys^{335} was ubiquitinated (Fig. 2*C*). To confirm the contribution of Lys^{335} to the ubiquitination-mediated down-regulation of MHC I, we made another mutant in which Lys^{335} was mutated to arginine but the other lysines were left intact (K335R). As shown in supplemental Fig. S2, this mutant was not significantly down-regulated or ubiquitinated by MIR2. These results demonstrate that ubiquitination at Lys^{335} is important for the down-regulation of MHC I by MIR2.

These results strongly suggest that surface-expressed CD8-MHC I is internalized as a result of ubiquitination. To confirm this, we repeated the FACS analysis as performed in Figs. 1*D* and 2*C*, but within a shorter time frame, 10 min, which is before the endocytic events take place. Also, we examined whether polyubiquitination or monoubiquitination could induce internalization of CD8-MHC I more efficiently. To make a monoubiquitinated molecule, we constructed a ubiquitin-fused CD8 chimera (termed K-less-UbiK0), in which a lysine-less ubiquitin (UbiK0) was fused to the C-terminal portion of CD8-MHC I-K-less (Fig. 3*A*). As shown in Fig. 3*B*, surface-expressed Lys^{335} was significantly down-regulated within the first 5 min, but only when MIR2 was expressed. By contrast, surface-expressed CD8-MHC I-K-less was not down-regulated at all within the first 5 or 10 min even in the presence of MIR2. The monoubiquitinated CD8-MHC I (K-less-UbiK0) was only slightly down-regulated by 10 min, and moreover this down-regulation occurred to an equivalent extent in the presence or absence of Dox (Fig. 3*B*). These data

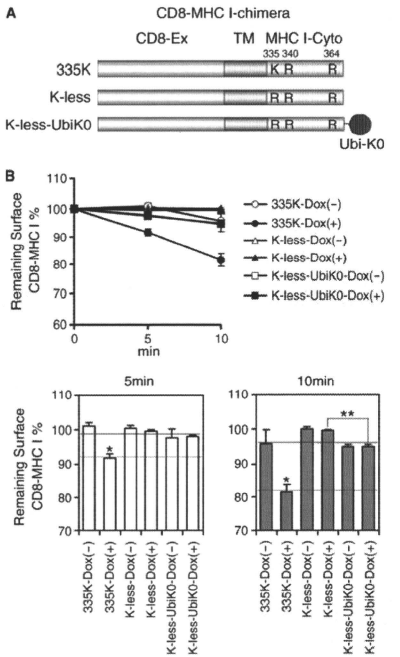

FIGURE 3. **Polyubiquitination is necessary for efficient CD8-MHC I internalization.** *A*, schematic representation of the CD8-chimera fusion proteins used in this study is shown. The extracellular region of CD8 (*CD8-Ex*) and the transmembrane (*TM*) and cytoplasmic regions of MHC I (*MHC I-Cyto*) are indicated. *B*, surface CD8 chimeras were labeled with anti-CD8 Ab after the cells were incubated with (+) or without (−) Dox for 24 h. After cultivation at 37 °C for the indicated times, the expression of the remaining surface CD8 chimera was examined as in Fig. 1*D*. At each time point, the percentage of remaining CD8 chimera was calculated relative to the value at 0 min (*lower panel*). The values are mean ± S.E. (*error bars*) ($n = 3$); *, $p < 0.05$ compared with 335K-Dox(−), K-less-Dox(− or +) and K-less-UbiK0-Dox(− or +). **, $p < 0.05$ K-less-UbiK0-Dox(+) was compared with K-less-Dox(+).

indicate that polyubiquitination serves as a better internalization signal than monoubiquitination in the context of MIR2. Therefore, T-REx-MIR2 cells and the CD8-MHC I chimera together provide a suitable experimental system to study how MHC I internalization is regulated by its polyubiquitination.

Epsin1 Is an Adaptor Molecule for MHC I Internalization by MIR2—We next examined how MIR2 induces the internalization of MHC I. Recently, several adaptor molecules (epsin1, EPS15, and EPS15R) have been shown to mediate the interaction between ubiquitinated cargo molecules and clathrin, which is an inducer of internalization (7, 9). We first examined the contribution of clathrin to MIR2-mediated internalization. As shown in supplemental Fig. S3, siRNA-mediated clathrin depletion blocked the down-regulation of CD8-MHC I even though CD8-MHC I was still ubiquitinated. Next, the binding of epsin1, EPS15, and EPS15R to ubiquitinated MHC I was examined. As shown in Fig. 4*A* and supplemental Fig. S3*F*, the CD8-MHC I molecules internalized as a result of MIR2-mediated ubiquitination associated efficiently with epsin1, but not with EPS15 or EPS15R. To confirm the association between the UIM domains of epsin1 and the ubiquitinated MHC I, several epsin1 mutants were coexpressed in HeLa cells with MIR2 and CD8-MHC I containing only the Lys^{335} ubiquitination site in its cytoplasmic tail (CD8-MHC I 335K). All UIMs-containing epsin1 molecules interacted with polyubiquitinated CD8-MHC I (Fig. 4*C*), and similar results were obtained with endogenous MHC I (supplemental Fig. S4). Because K-less-UbiK0 showed some slight internalization as seen in Fig. 3*B*, we also examined whether epsin1 could associate with this monoubiquitinated CD8-MHC I and found that it did not (supplemental Fig. S5). These results suggest that epsin1 interacts with polyubiquitinated MHC I more strongly than with monoubiquitinated MHC I and functions as an adaptor molecule for MIR2-mediated internalization.

To test this hypothesis further, we inhibited the expression of epsin1 by siRNA in MIR2-expressing HeLa cells (HeLa-MIR2; Fig. 4*D*), which have low level expression of MHC I because of its enhanced internalization. The siRNA-mediated inhibition of epsin1 rescued the surface expression of MHC I by blocking its internalization (Fig. 4*D*), and the same result was obtained with CD8-MHC I 335K (supplemental Fig. S6). To confirm that the association between epsin1 and ubiquitinated MHC I is necessary for MHC I internalization, we attempted to disrupt this association by using epsin1 dominant negative mutants. We reasoned that if the association requires the epsin1 UIM, then expression of a UIM-deletion mutant of epsin1 (ΔUIM) might disrupt it. As expected, the association between ubiquitinated CD8-MHC I 335K and endogenous epsin1 was inhibited, and the down-regulation of CD8-MHC I was prevented by ΔUIM (supplemental Fig. S7). Taken together, these results strongly suggest that recognition of ubiquitin chains by the epsin1 UIMs is important for polyubiquitination-enhanced MHC I internalization.

Generation of a Lys^{11} and Lys^{63} Mixed-linkage Ubiquitin Chain at Lys^{335}—Several atypical ubiquitin chains have been reported to be novel signal mediators (14, 15, 19); therefore, we examined the composition of the ubiquitin chain(s) that induce the internalization of MHC I. Because we found that epsin1 is a functional adaptor for the polyubiquitin chain generated on MHC I, we purified ubiquitin chains associated with epsin1 from denatured CD8-MHC I 335K and analyzed them by mass spectrometry. As shown in Fig. 5*A*, among the seven possible linkages, the Lys^{63} linkage was most strongly detected, but interestingly, the Lys^{11} linkage was also readily detectable. Similar results were obtained with endogenous MHC I polyubiquitinated by MIR2 (supplemental Fig. S8). Based on these results, two possible scenarios can be envisioned: either each MHC I molecule receives a pure Lys^{11}-linked or a pure Lys^{63}-linked polyubiquitin chain at Lys^{335}, or each MHC I molecule receives a single polyubiquitin chain consisting of both Lys^{11} and Lys^{63} linkages.

To discriminate between these two possibilities, we examined how mutant ubiquitin modifies the formation of the polyubiquitin chains generated at Lys^{335}. The indicated mutant

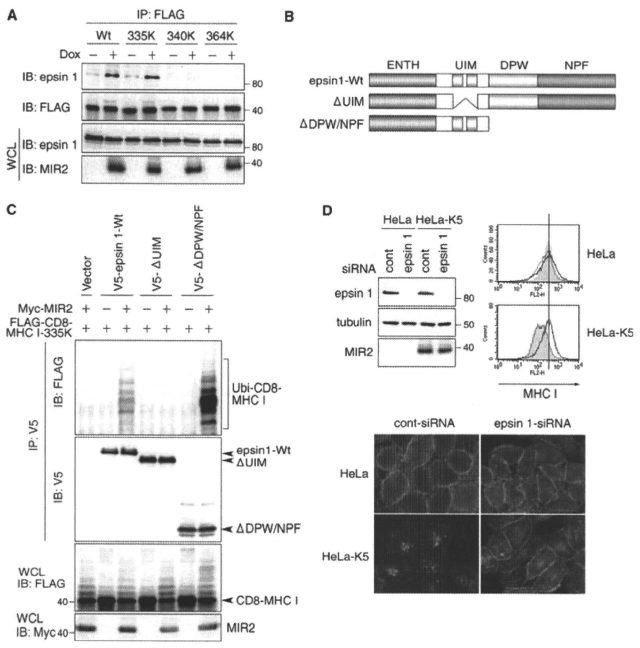

FIGURE 4. **Epsin1 is an adaptor molecule for MIR2-mediated MHC I internalization.** *A*, after incubation with or without Dox for 6 h, protein complexes that included the indicated CD8-MHC I chimeras were isolated from the indicated CD8-MHC I-expressing T-REx-MIR2 cells. The purified protein complexes were examined with anti-epsin1 Ab or M2 Ab. *B*, schematic representation of the epsin1 mutants used in this study is shown. The UIM, DPW domain, NPF domain, and epsin N-terminal homology domain (*ENTH*) are indicated. *C*, each indicated V5-tagged epsin1 was coexpressed with CD8-MHC I 335K and MIR2 in HeLa cells. Protein complexes that included each exogenous epsin1 were purified with anti-V5 Ab and analyzed by Western blotting with M2 and V5 Ab. The expression of CD8-MHC I 335K and MIR2 was examined in whole cell lysates with M2 Ab and anti-Myc Ab, respectively. *D*, control siRNA (scrambled) or siRNA for epsin1 was transfected into HeLa or MIR2-expressing HeLa cells. Whole cell lysates from the indicated cells were analyzed with anti-epsin1 and anti-tubulin Abs. The expression of MHC I in the indicated HeLa cells was examined by flow cytometry. The *gray histogram* indicates MHC I expression in nontransfected HeLa cells. The dotted line indicates the MHC I expression in control siRNA-transfected HeLa cells. The *solid line* indicates the MHC I expression in epsin1 siRNA-transfected HeLa cells. In the *lower panel*, the indicated transfected cells were cultivated with anti-MHC I Ab (W6/32) for 10 min. Internalized MHC I was observed by fluorescence microscopy as in Fig. 1*D*.

ubiquitin was coexpressed with CD8-MHC I 335K and MIR2 in HeLa cells (Fig. 5*B*). To monitor the expression of the mutant ubiquitin, the wild-type or mutant protein was fused to the N terminus of GFP. Each GFP-tagged ubiquitin was cleaved at its junction with GFP, and the resultant free GFP was used as an indicator of ubiquitin expression. Ubiquitin in which Lys^{11} and/or Lys^{63} was mutated to arginine inhibited the generation of polyubiquitin chains (Fig. 5*B*). By contrast, ubiquitin in which Lys^{48} or Lys^{29} was mutated to arginine had no effect on this process. Ubi-K11R significantly inhibited the generation of polyubiquitinated bands with molecular weights greater than that of Ubi_4-CD8-MHC I, and the inhibitory effect of this mutant depended on its expression level (supplemental Fig. S9). However, Ubi-K63R significantly inhibited the generation of polyubiquitinated bands with molecular weights greater than that of Ubi_2-CD8-MHC I (Fig. 5*B*). The significance of these data was confirmed statistically (supplemental Fig. S10). These results suggest that a single Lys^{11} and Lys^{63} mixed-linkage chain is generated on MHC I and that in this mixed chain, Lys^{63} linkages and Lys^{11} linkages are present in the proximal and distal regions, respectively.

To test this hypothesis further, we examined two ubiquitinated CD8-MHC I 335K bands of different lengths: Ubi_2-CD8-MHC I and Ubi_4-CD8-MHC I (Fig. 5*C*). As expected, Ubi_2-CD8-MHC I mainly consisted of Lys^{63} linkages, whereas Ubi_4-CD8-MHC I mainly consisted of Lys^{11} and Lys^{63} linkages. A monoclonal antibody is now available that specifically detects Lys^{63} linkages (35). Therefore, we used Western blot analysis to confirm that both Ubi-K11R and Ubi-K63R inhibit the formation of Lys^{63} linkages. Ubi-K11R inhibited the generation of Lys^{63}-linkage-containing polyubiquitinated bands with molecular weights greater than that of Ubi_4-CD8-MHC I, and Ubi-K63R inhibited the generation of Lys^{63}-linkage-containing polyubiquitinated bands with molecular weights greater than that of Ubi_2-CD8-MHC I (Fig. 5*D*). Taken together, these data provide strong evidence that a Lys^{11} and Lys^{63} mixed-linkage ubiquitin chain is generated at Lys^{335} of MHC I and that this unusual chain contributes to the internalization of MHC I by MIR2.

MHC I Internalization by Lys^{11} and Lys^{63} Mixed-linkage Ubiquitin Chains—To examine whether a Lys^{11} and Lys^{63} mixed-linkage chain functions as internalization signal for MHC I, we expressed GFP-tagged ubiquitin mutants in MIR2-expressing BJAB cells. MIR2-expressing cells express lower levels of cell surface MHC I compared with the parental BJAB cells (Fig. 6*A*). As we expected, ubiquitins in which Lys^{11} and/or Lys^{63} were mutated to arginine inhibited the down-regulation of MHC I in cells in which transfected ubiquitin was highly expressed, as assessed by EGFP expression (shown by the *rectangles* in the *upper right quadrants* of Fig. 6*A*), whereas the wild type and the Lys^{48} ubiquitin mutants did not (Fig. 6*A*). To evaluate this phenomenon more quantitatively, we measured the surface expression levels of MHC I in low and high GFP-expressing cell populations and calculated the ratios of these two values (Fig. 6*B*, *upper panel*).

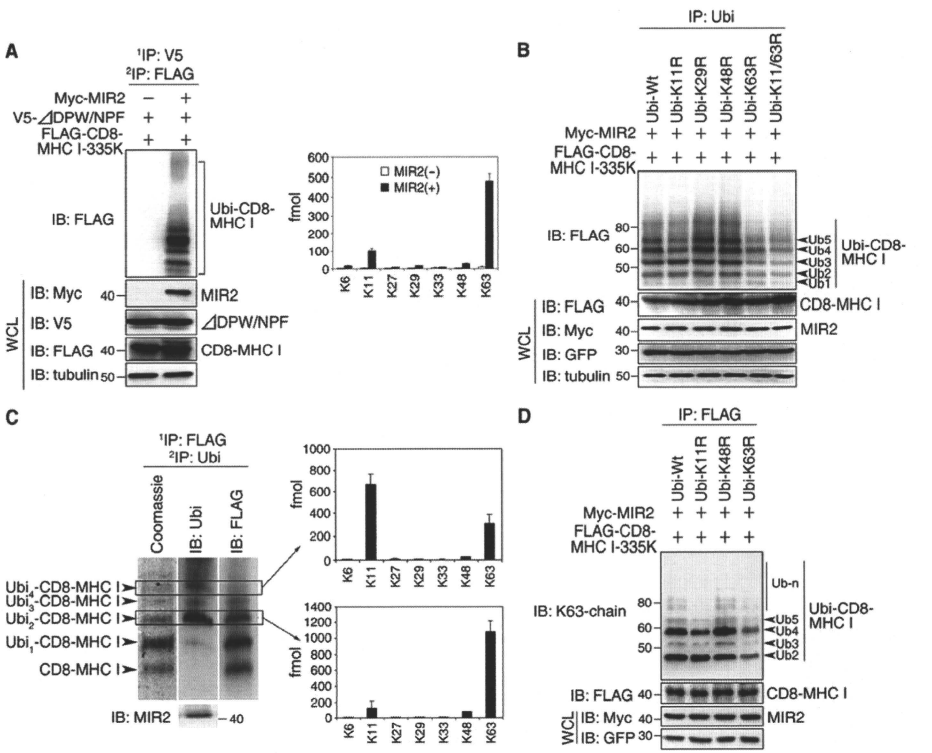

FIGURE 5. **Generation of the Lys^{11} and Lys^{63} mixed-linkage ubiquitin chain at Lys^{335}.** *A*, CD8-MHC I 335K and V5-tagged epsin1 were coexpressed in HeLa cells with (MIR2(+)) or without MIR2 (MIR2(−)). First, the protein complex containing ubiquitinated CD8-MHC I 335K and epsin1 was purified with an anti-V5 Ab and denatured by boiling in 2% SDS buffer. The denatured, CD8-MHC I 335K was then purified with an anti-FLAG M2 Ab. After confirmation by Western blot analysis (*left panel*), each sample was analyzed by mass spectrometry (*right panel*). *B*, each indicated EGFP-tagged ubiquitin was coexpressed with CD8-MHC I 335K and MIR2 in HeLa cells. The ubiquitinated form of CD8-MHC I 335K was purified with the FK2 Ab and examined with the M2 Ab. Equal amounts of CD8-MHC I 335K were analyzed in all samples. *C*, the ubiquitinated forms of CD8-MHC I were sequentially purified from T-REx-MIR2 cells with M2 Ab and FK2 Ab and separated by SDS-PAGE. After confirmation by Western blot analysis with the indicated Abs, the peptides obtained from the bands indicated by the *rectangle* were analyzed by LC-MS/MS. *D*, each indicated EGFP-tagged ubiquitin was coexpressed with CD8-MHC I 335K and MIR2 in HeLa cells. The ubiquitinated form of CD8-MHC I 335K was purified with the M2 Ab and examined with the Lys^{63} linkage-specific Ab, Apu3. Equal amounts of CD8-MHC I 335K were analyzed in all samples.

The significance of the inhibition of the down-regulation of MHC I surface expression by each ubiquitin mutant was confirmed statistically (Fig. 6*B*, *lower panel*). As expected, neither the Lys^{29} nor the Lys^{33} ubiquitin mutants rescued MIR2-mediated MHC I down-regulation (Fig. 6*A*). The same results were obtained with CD8-MHC I 335K (supplemental Fig. S11). Next, we examined whether blocking Lys^{11}- or Lys^{63}-linked ubiquitination suppressed the internalization of MHC I in MIR2-expressing BJAB cells. First, we analyzed the down-regulation of surface-expressed MHC I in cells that highly expressed the indicated ubiquitin molecules at the indicated times and found that both Ubi-K11R and Ubi-K63R inhibited the down-regulation of surface-expressed MHC I (Fig. 6*C*). To examine whether this down-regulation was due to inhibition of internalization, we analyzed the down-regulation of surface-expressed MHC I within the first 10 min as performed in Fig. 3*B*. As shown in Fig. 6*D*, both Ubi-K11R and Ubi-K63R inhibited the down-regulation of surface-expressed MHC I within this time frame, indicating that a Lys^{11} and Lys^{63} mixed-linkage polyubiquitin chain is required for MHC I internalization.

The next important question was how do these Lys^{11} and Lys^{63} linkages contribute to the interaction between the mixed polyubiquitin chain and epsin1. After confirmation of the association between a Lys^{11} and Lys^{63} mixed-linkage chain and epsin1 by inhibiting chain formation with Ubi-K63R (supplemental Fig. S12), we examined the interaction between pure

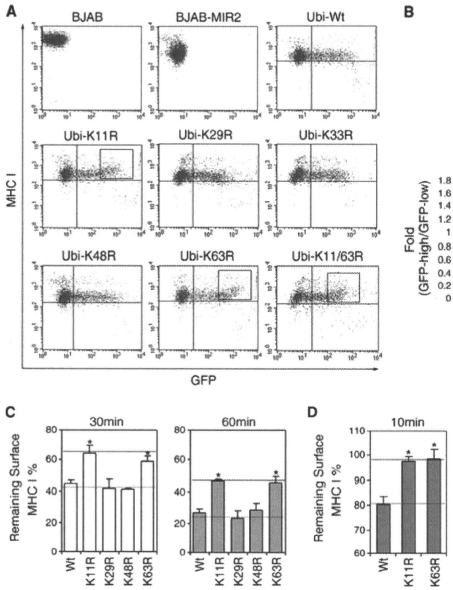

FIGURE 6. **Contribution of the Lys^{11} and Lys^{63} mixed-linkage ubiquitin chain to protein internalization.** *A*, each indicated EGFP-tagged ubiquitin was expressed in constitutively MIR2-expressing BJAB cells. Two days after the introduction of each exogenous ubiquitin by electroporation, the expression level of MHC I was examined by flow cytometry. *B*, the surface expression levels of MHC I in low GFP-expressing and high GFP-expressing cell populations were measured as indicated in the *upper panel*, and the ratios of these two values are shown in the *lower panel*. The values are mean ± S.E. (*error bars*) ($n = 3$); *, $p < 0.01$ compared with wild-type ubiquitin (*Wt*). *C*, after each EGFP-tagged ubiquitin was expressed as in *A*, the down-regulation of surface MHC I at the indicated time points was examined in the cell population in which EGFP was highly expressed, as in Fig. 1*D*. The values are mean ± S.E. ($n = 3$); *, $p < 0.01$ compared with wild-type ubiquitin. *D*, the same experiment as in *C* was performed at a different time point (10 min). The values are mean ± S.E. ($n = 3$); *, $p < 0.01$ compared with wild-type ubiquitin.

Lys^{11}- or pure Lys^{63}-linked polyubiquitin chains and a glutathione *S*-transferase (GST) fusion protein containing the UIM domains of epsin1 (GST-UIM). The pure Lys^{63}-linked polyubiquitin chain, but not the pure Lys^{11}-linked polyubiquitin chain, interacted with GST-UIM (supplemental Fig. S13). This result suggests that the Lys^{11} linkages do not directly contribute to the binding to epsin1.

DISCUSSION

It has been reported that protein ubiquitination is an important signal for receptor internalization from the cell surface (6–10). However, it is still unclear how a polyubiquitin chain regulates the internalization step because it has been shown that monoubiquitination is sufficient to induce receptor internalization in yeast (11, 12). By use of the Tet-on expression system for MIR2 and quantitative mass spectrometry, we demonstrated that the polyubiquitin chain generated by MIR2 is a Lys^{11} and Lys^{63} mixed-linkage chain that is required for efficient epsin1-dependent internalization of MHC I. Given that it has recently been reported that the Lys^{11}-linked polyubiquitin chain is a signal for proteasomal degradation involved in anaphase-promoting complex-mediated cell-cycle control and in endoplasmic reticulum-associated degradation (18, 19), our findings provide further evidence that atypical polyubiquitin chains have specific functions *in vivo*.

Previous studies of how polyubiquitination contributes to internalization were performed with polyubiquitin chains generated at multiple ubiquitin acceptor sites in the target membrane proteins, making it very difficult to analyze the function of a single polyubiquitin chain. We were able to define a single polyubiquitin chain consisting of mixed Lys^{11} and Lys^{63} linkages by using a MHC I mutant with only one lysine, Lys^{335}, as the ubiquitin acceptor site. In addition, we found that both lysine residues (Lys^{335} and Lys^{340}) in the cytosolic tail in MHC I are ubiquitinated, but only the ubiquitination at Lys^{335} contributes to efficient internalization. Thus, the experimental system reported in this study may be useful for further investigation of how the quality of ubiquitination (*e.g.* ubiquitin acceptor site of the substrate, ubiquitin linkage) contributes to internalization *in vivo*.

In this report, we demonstrated that a Lys^{11} and Lys^{63} mixed-linkage chain generated by MIR2 is required for internalization of MHC I. These results are consistent with the findings recently reported by Boname *et al.* (36). Furthermore, we found that this novel polyubiquitin chain can function as an internalization signal for MHC I through its association with epsin1, an adaptor molecule containing a UIM domain. Therefore, an important next question is how the Lys^{11}/Lys^{63} mixed-linkage chain is recognized by the UIM domains. Recently, it has been reported that the UIM domains of epsin1 bind preferentially to Lys^{63}-linked rather than Lys^{48}-linked ubiquitin chains (20) because the inter-UIM region forms a 12-Å-long α-helix. This structure ensures that the UIMs are spatially arranged to allow specific binding to Lys^{63}-linked diubiquitin. Moreover, using molecular modeling of ubiquitin, Lys^{11}-linked chains are predicted to form a closed conformation similar to that in Lys^{48}-linked chains (37), whereas Lys^{63}-linked chains adopt a highly open conformation (38). Consistent with these findings, we observed that the UIM domains of epsin1 associate with Lys^{63}-linked chains, but not with Lys^{11}-linked chains, suggesting that the Lys^{11} linkages generated by MIR2 may not directly contribute to interaction with epsin1.

The most plausible model at this point is that epsin1 binds to a Lys^{63}-linked diubiquitin and longer chains and that the presence of Lys^{11} (either as a mixed chain, as a cap, or as a side branch) facilitates some events related to Ub-dependent endocytosis. The Lys^{11} linkages might support the extension of the polyubiquitin chain required for efficient internalization, or they might generate a suitable chain topology to promote the association between Lys^{63} linkages and epsin1 *in vivo*. Also, Lys^{11} linkages may interact with a second ubiquitin-interacting protein that is needed for endocytosis and/or subsequent sorting. Further intensive experiments are needed to test these hypotheses.

Previous studies have focused exclusively on the contribution of the Lys^{63} linkage to internalization and lysosomal degradation (8, 39, 40), a reasonable approach because no significant amounts of Lys^{11}-linked chains, compared with Lys^{48}- or Lys^{63}-linked chains, had been observed (40, 41). Therefore, we examined whether Lys^{11} and Lys^{63} linkages are present in polyubiquitin chains generated on substrates (*e.g.* B7-2) ubiquitinated by other MIR family members. Quantitative mass spectrometric analysis indicates that indeed there are both Lys^{11} linkages and Lys^{63} linkages in the polyubiquitin chains generated on these substrates.[3] Although further analysis is required, it now seems plausible that Lys^{11} and Lys^{63} mixed-polyubiquitin chains are a common internalization signal utilized by MIR family members.

Acknowledgments—We thank H. Ploegh for HC10 antibody, K. Umebayashi for the EGFP-Ubi-expressing plasmid, P. Burrows for critical reading of the manuscript, and S. Dohi for manuscript preparation.

REFERENCES

1. Raiborg, C., and Stenmark, H. (2009) *Nature* **458,** 445–452
2. Shtiegman, K., Kochupurakkal, B. S., Zwang, Y., Pines, G., Starr, A., Vexler, A., Citri, A., Katz, M., Lavi, S., Ben-Basat, Y., Benjamin, S., Corso, S., Gan, J., Yosef, R. B., Giordano, S., and Yarden, Y. (2007) *Oncogene* **26,** 6968–6978
3. Gay, D. L., Ramón, H., and Oliver, P. M. (2008) *Immunol. Res.* **42,** 51–64
4. Gómez-Martín, D., Díaz-Zamudio, M., and Alcocer-Varela, J. (2008) *Autoimmun. Rev.* **7,** 284–290
5. Roepstorff, K., Grøvdal, L., Grandal, M., Lerdrup, M., and van Deurs, B. (2008) *Histochem. Cell Biol.* **129,** 563–578
6. Geetha, T., Jiang, J., and Wooten, M. W. (2005) *Mol. Cell* **20,** 301–312
7. Barriere, H., Nemes, C., Lechardeur, D., Khan-Mohammad, M., Fruh, K., and Lukacs, G. L. (2006) *Traffic* **7,** 282–297
8. Duncan, L. M., Piper, S., Dodd, R. B., Saville, M. K., Sanderson, C. M., Luzio, J. P., and Lehner, P. J. (2006) *EMBO J.* **25,** 1635–1645
9. Traub, L. M., and Lukacs, G. L. (2007) *J. Cell Sci.* **120,** 543–553
10. Varghese, B., Barriere, H., Carbone, C. J., Banerjee, A., Swaminathan, G., Plotnikov, A., Xu, P., Peng, J., Goffin, V., Lukacs, G. L., and Fuchs, S. Y. (2008) *Mol. Cell. Biol.* **28,** 5275–5287
11. Dupré, S., Urban-Grimal, D., and Haguenauer-Tsapis, R. (2004) *Biochim. Biophys. Acta* **1695,** 89–111
12. Acconcia, F., Sigismund, S., and Polo, S. (2009) *Exp. Cell Res.* **315,** 1610–1618
13. Hershko, A., and Ciechanover, A. (1998) *Annu. Rev. Biochem.* **67,** 425–479
14. Ikeda, F., and Dikic, I. (2008) *EMBO Rep.* **9,** 536–542
15. Adhikari, A., and Chen, Z. J. (2009) *Dev. Cell* **16,** 485–486
16. Chastagner, P., Israël, A., and Brou, C. (2006) *EMBO Rep.* **7,** 1147–1153
17. Ikeda, H., and Kerppola, T. K. (2008) *Mol. Biol. Cell* **19,** 4588–4601
18. Williamson, A., Wickliffe, K. E., Mellone, B. G., Song, L., Karpen, G. H., and Rape, M. (2009) *Proc. Natl. Acad. Sci. U.S.A.* **106,** 18213–18218
19. Xu, P., Duong, D. M., Seyfried, N. T., Cheng, D., Xie, Y., Robert, J., Rush, J., Hochstrasser, M., Finley, D., and Peng, J. (2009) *Cell* **137,** 133–145
20. Sato, Y., Yoshikawa, A., Mimura, H., Yamashita, M., Yamagata, A., and Fukai, S. (2009) *EMBO J.* **28,** 2461–2468
21. Itoh, T., Koshiba, S., Kigawa, T., Kikuchi, A., Yokoyama, S., and Takenawa, T. (2001) *Science* **291,** 1047–1051
22. Owen, D. J., Vallis, Y., Noble, M. E., Hunter, J. B., Dafforn, T. R., Evans, P. R., and McMahon, H. T. (1999) *Cell* **97,** 805–815
23. Wang, H., Traub, L. M., Weixel, K. M., Hawryluk, M. J., Shah, N., Edinger, R. S., Perry, C. J., Kester, L., Butterworth, M. B., Peters, K. W., Kleyman, T. R., Frizzell, R. A., and Johnson, J. P. (2006) *J. Biol. Chem.* **281,** 14129–14135
24. Hawryluk, M. J., Keyel, P. A., Mishra, S. K., Watkins, S. C., Heuser, J. E., and Traub, L. M. (2006) *Traffic* **7,** 262–281
25. Goto, E., Mito-Yoshida, M., Uematsu, M., Aoki, M., Matsuki, Y., Ohmura-Hoshino, M., Hotta, H., Miyagishi, M., and Ishido, S. (2008) *PLoS ONE* **3,** e1490
26. Ishido, S., Goto, E., Matsuki, Y., and Ohmura-Hoshino, M. (2009) *Curr. Opin. Immunol.* **21,** 78–83
27. Kirkpatrick, D. S., Denison, C., and Gygi, S. P. (2005) *Nat. Cell Biol.* **7,** 750–757
28. Kirkpatrick, D. S., Hathaway, N. A., Hanna, J., Elsasser, S., Rush, J., Finley, D., King, R. W., and Gygi, S. P. (2006) *Nat. Cell Biol.* **8,** 700–710
29. Umebayashi, K., Stenmark, H., and Yoshimori, T. (2008) *Mol. Biol. Cell* **19,** 3454–3462
30. Ishido, S., Wang, C., Lee, B. S., Cohen, G. B., and Jung, J. U. (2000) *J. Virol.* **74,** 5300–5309
31. Lehner, P. J., Hoer, S., Dodd, R., and Duncan, L. M. (2005) *Immunol. Rev.* **207,** 112–125
32. Ohmura-Hoshino, M., Goto, E., Matsuki, Y., Aoki, M., Mito, M., Uematsu, M., Hotta, H., and Ishido, S. (2006) *J. Biochem.* **140,** 147–154
33. Coscoy, L., Sanchez, D. J., and Ganem, D. (2001) *J. Cell Biol.* **155,** 1265–1273
34. Hicke, L., and Dunn, R. (2003) *Annu. Rev. Cell Dev. Biol.* **19,** 141–172
35. Newton, K., Matsumoto, M. L., Wertz, I. E., Kirkpatrick, D. S., Lill, J. R., Tan, J., Dugger, D., Gordon, N., Sidhu, S. S., Fellouse, F. A., Komuves, L., French, D. M., Ferrando, R. E., Lam, C., Compaan, D., Yu, C., Bosanac, I., Hymowitz, S. G., Kelley, R. F., and Dixit, V. M. (2008) *Cell* **134,** 668–678
36. Boname, J. M., Thomas, M., Stagg, H. R., Xu, P., Peng, J., and Lehner, P. J. (2010) *Traffic* **11,** 210–220
37. Fushman, D., and Walker, O. (2010) *J. Mol. Biol.* **395,** 803–814
38. Komander, D., Reyes-Turcu, F., Licchesi, J. D., Odenwaelder, P., Wilkinson, K. D., and Barford, D. (2009) *EMBO Rep.* **10,** 466–473
39. Barriere, H., Nemes, C., Du, K., and Lukacs, G. L. (2007) *Mol. Biol. Cell* **18,** 3952–3965
40. Kumar, K. G., Barriere, H., Carbone, C. J., Liu, J., Swaminathan, G., Xu, P., Li, Y., Baker, D. P., Peng, J., Lukacs, G. L., and Fuchs, S. Y. (2007) *J. Cell Biol.* **179,** 935–950
41. Tanaka, Y., Tanaka, N., Saeki, Y., Tanaka, K., Murakami, M., Hirano, T., Ishii, N., and Sugamura, K. (2008) *Mol. Cell Biol.* **28,** 4805–4818

[3] E. Goto, Y. Yamanaka, A. Ishikawa, M. Aoki-Kawasumi, M. Mito-Yoshida, M. Ohmura-Hoshino, Y. Matsuki, M. Kajikawa, H. Hirano, and S. Ishido, unpublished data.

Science Signaling
AAAS

AAA+ Proteins RUVBL1 and RUVBL2 Coordinate PIKK Activity and Function in Nonsense-Mediated mRNA Decay

Natsuko Izumi, Akio Yamashita, Akihiro Iwamatsu, Rie Kurata, Hiroki Nakamura, Bonnie Saari, Hisashi Hirano, Philip Anderson and Shigeo Ohno (6 April 2010)
Science Signaling **3** (116), ra27. [DOI: 10.1126/scisignal.2000468]

Science Signaling (ISSN 1937-9145) is published weekly, except the last week in December, by the American Association for the Advancement of Science, 1200 New York Avenue, NW, Washington, DC 20005.

MOLECULAR BIOLOGY

AAA+ Proteins RUVBL1 and RUVBL2 Coordinate PIKK Activity and Function in Nonsense-Mediated mRNA Decay

Natsuko Izumi,[1] Akio Yamashita,[1,2,6*] Akihiro Iwamatsu,[3] Rie Kurata,[1] Hiroki Nakamura,[4] Bonnie Saari,[5] Hisashi Hirano,[4] Philip Anderson,[5] Shigeo Ohno[1,6*]

(Published 6 April 2010; Volume 3 Issue 116 ra27)

Phosphatidylinositol 3-kinase–related protein kinase (PIKK) family proteins play essential roles in DNA-based and RNA-based processes, such as the response to DNA damage, messenger RNA (mRNA) quality control, transcription, and translation, where they contribute to the maintenance of genome integrity and accurate gene expression. The adenosine triphosphatases associated with diverse cellular activities (AAA+) family proteins RuvB-like 1 (RUVBL1) and RUVBL2 are involved in various cellular processes, including transcription, RNA modification, DNA repair, and telomere maintenance. We show that RUVBL1 and RUVBL2 associate with each PIKK family member. We also show that RUVBL1 and RUVBL2 control PIKK abundance at least at the mRNA level. Knockdown of RUVBL1 or RUVBL2 decreased PIKK abundance and impaired PIKK-mediated signaling. Analysis of SMG-1, a PIKK family member involved in nonsense-mediated mRNA decay (NMD), revealed an essential role for RUVBL1 and RUVBL2 in NMD. RUVBL1 and RUVBL2 associated with SMG-1 and the messenger ribonucleoproteins in the cytoplasm and promoted the formation of mRNA surveillance complexes during NMD. Thus, RUVBL1 and RUVBL2 regulate PIKK functions on two different levels: They control the abundance of PIKKs and they stimulate the formation of PIKK-containing molecular complexes, such as those involved in NMD.

INTRODUCTION

Phosphatidylinositol 3-kinase (PI3K)–related protein kinases (PIKKs) are unconventional serine–threonine protein kinases, and their catalytic domains are homologous to the catalytic domains of phosphatidylinositol 3-kinases. The PIKK family in mammals includes the following catalytically active members, DNA-PKcs (DNA-dependent protein kinase catalytic subunit), ATM (ataxia telangiectasia mutated), ATR (ATM- and Rad3-related), mTOR (mammalian target of rapamycin), SMG-1 (suppressor with morphogenetic effect on genitalia-1), as well as the catalytically inactive member TRRAP (transformation/transcription domain–associated protein) (*1*, *2*). PIKKs are large molecules (270 to 470 kD) with a conserved kinase domain, a FAT-C (FRAP, ATM, TRRAP C-terminal) domain, and multiple helical repeats (*1*, *3*). ATM, ATR, TRRAP, and mTOR are evolutionarily conserved from *Saccharomyces cerevisiae* to *Homo sapiens*, whereas DNA-PKcs and SMG-1 appeared during metazoan evolution. DNA-PKcs, ATM, ATR, and SMG-1 sense the DNA damage and activate effector proteins to induce cell cycle arrest and DNA repair pathways (*4*–*7*). SMG-1 also detects premature termination codons (PTCs) and activates the messenger RNA (mRNA) surveillance complex to induce degradation of mRNAs with PTCs (*8*). mTOR senses nutrient status and controls cell growth and proliferation and protein translation (*9*). TRRAP is involved in transcription and DNA repair as a core component of a histone acetyltransferase (HAT) complex (*10*). Thus, PIKKs function in controlling accurate gene expression through their roles in surveillance of the integrity of genome and transcripts, as well as function to control protein production in response to nutrient supply.

SMG-1 is part of a multiprotein complex called SMG1C that is composed of SMG-1, SMG-8, and SMG-9 (*11*). SMG1C is essential for nonsense-mediated mRNA decay (NMD), an mRNA quality control mechanism that occurs in the cytoplasm and detects and degrades mRNAs with PTC, to prevent the production of potentially harmful C-terminally truncated proteins (*8*, *12*–*14*). In mammals, PTC recognition involves sequential remodeling of the mRNA surveillance complex on messenger ribonucleoproteins (mRNPs), which contain the nuclear cap-binding proteins CBP20 and CBP80 and the cytoplasmic poly(A)-binding protein PABPC1. During the initial round of translation, a termination complex, called the SURF complex forms at the site of a PTC-recognizing ribosome. SURF is so named because this complex contains SMG-1, Upf1, and the eukaryotic release factors (eRFs), eRF1 and eRF3. If a cytoplasmic exon-junction complex (EJC; a protein complex deposited 20 to 24 nucleotides upstream of an exon-exon junction and composed of Upf2, Upf3b, eIF4A3, Y14, Magoh, and Btz) is present downstream from the termination codon, the ribosome-SURF complex binds to the EJC to form a DECID (decay-inducing) complex, which triggers SMG-1–mediated phosphorylation of Upf1, an essential process in NMD (*8*, *11*, *12*, *15*). In addition to its roles in NMD and DNA damage responses (*7*), SMG-1 may also have an antiapoptotic function that is triggered in response to a tumor necrosis factor–α (TNF-α) (*16*).

RUVBL1 and RUVBL2, also known as TIP49a and TIP49b or Pontin and Reptin, are closely related AAA+ [ATPases (adenosine triphosphatases) associated with diverse cellular activities] family proteins (*17*). Both RUVBL1 and RUVBL2 have ATPase and DNA helicase activities in vitro (*18*). Together, RUVBL1 and RUVBL2 form a double hexamer (*19*–*21*) and function in various nuclear multimolecular complexes, including various chromatin-remodeling complexes, a HAT complex, and small nucleolar ribonucleoprotein (snoRNP) complexes, and the telomerase

[1]Department of Molecular Biology, Yokohama City University School of Medicine, Yokohama 236-0004, Japan. [2]Precursory Research for Embryonic Science and Technology (PRESTO), Japan Science and Technology Agency, Kawaguchi 332-0012, Japan. [3]Protein Research Network Co., Ltd., Yokohama 236-0004, Japan. [4]International Graduate School of Arts and Sciences, Yokohama City University, Yokohama 230-0045, Japan. [5]Department of Genetics, University of Wisconsin, Madison, WI 53706, USA. [6]Advanced Medical Research Center, Yokohama City University, Yokohama 236-0004, Japan.
*To whom correspondence should be addressed. E-mail: ohnos@med.yokohama-cu.ac.jp (S.O.); yamasita@yokohama-cu.ac.jp (A.Y.)

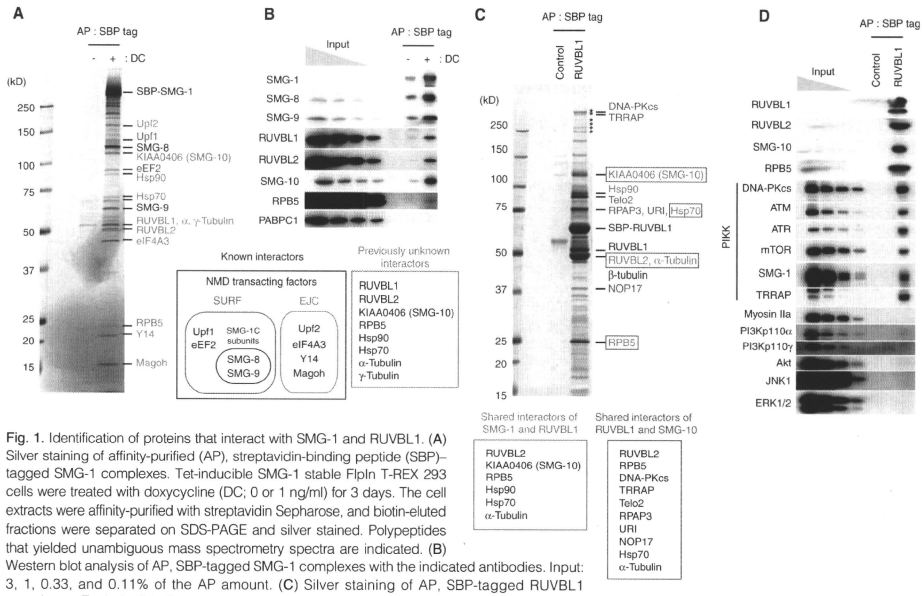

Fig. 1. Identification of proteins that interact with SMG-1 and RUVBL1. (**A**) Silver staining of affinity-purified (AP), streptavidin-binding peptide (SBP)–tagged SMG-1 complexes. Tet-inducible SMG-1 stable FlpIn T-REX 293 cells were treated with doxycycline (DC; 0 or 1 ng/ml) for 3 days. The cell extracts were affinity-purified with streptavidin Sepharose, and biotin-eluted fractions were separated on SDS-PAGE and silver stained. Polypeptides that yielded unambiguous mass spectrometry spectra are indicated. (**B**) Western blot analysis of AP, SBP-tagged SMG-1 complexes with the indicated antibodies. Input: 3, 1, 0.33, and 0.11% of the AP amount. (**C**) Silver staining of AP, SBP-tagged RUVBL1 complexes. Tet-inducible RUVBL1 stable FlpIn T-REX 293 cells or control cells, which express tag peptides only, were treated with DC (1 ng/ml) for 3 days. Samples were processed as in (A). Polypeptides that yielded unambiguous mass spectrometry spectra are indicated. All the identified proteins are listed in table S1. (**D**) Western blot analysis of AP, SBP-tagged RUVBL1 complexes with the indicated antibodies. Input: 1, 0.33, 0.11, and 0.037% of the AP amount. All experiments were performed three times, and typical results are shown.

reverse transcriptase complex (*22*–*24*). RUVBL1 and RUVBL2 regulate transcription by interacting with various transcription factors (*23*). Although RUVBL1 and RUVBL2 are predominantly nuclear proteins (*25*, *26*), they are also detectable in the cytoplasm (*27*), where their functions remain largely unknown.

In this study, we show that RUVBL1 and RUVBL2 associate with all PIKKs and regulate PIKK functions through two mechanisms, one at the level of the transcripts of PIKKs and one at the level of complex formation. We show that cells deficient in RUVBL1 or RUVBL2 exhibit decreased abundance of the PIKK transcripts and the encoded proteins. We also show that RUVBL1 and RUVBL2 play a critical role in the formation of the mRNA surveillance complex during NMD, through a mechanism that is independent of the effects of RUVBL1 and RUVBL2 on the abundance of SMG-1. These results suggest that RUVBL1 and RUVBL2 coordinate distinct PIKK functions and may serve to direct PIKKs to chromatin-based complexes or RNA-based complexes.

RESULTS

RUVBL1 and RUVBL2 associate with all PIKKs

To identify proteins that interact with SMG-1, we established a stable cell line that expresses SBP (streptavidin-binding peptide)-tagged SMG-1 (SBP-SMG-1) in a doxycycline-dependent manner. After purification of SBP-SMG-1, we identified the copurified proteins by mass spectrometry (Fig. 1A). These proteins included SMG1C subunits (SMG-8 and SMG-9) (*11*), NMD transacting factors (Upf1, Upf2, eIF4A3, Y14, and Magoh), a SURF-associated factor (eEF2), and molecular chaperones (Hsp90 and Hsp70). RUVBL1, RUVBL2, KIAA0406, and RPB5 were also identified as SMG-1–interacting proteins. RUVBL1 and RUVBL2 form a complex (RUVBL1/2) and function in various nuclear multiprotein complexes (*22*–*24*). *KIAA0406* is an uncharacterized gene encoding a putative protein of 1089 amino acids with no functional domains except for four HEAT (Huntingtin, elongation factor 3, A subunit of protein phosphatase 2A, and TOR1) repeats. Because R10H10.7, the *Caenorhabditis elegans* ortholog of KIAA0406, is involved in nematode NMD, we named KIAA0406 "SMG-10." RPB5 is a subunit of RNA polymerases I, II, and III (*28*). We confirmed the interactions between purified SBP-SMG-1 and RUVBL1, RUVBL2, SMG-10, and RPB5 by Western blotting (Fig. 1B).

We also investigated RUVBL1-interacting proteins with a similar strategy. Mass spectrometry identified SMG-10 and RPB5 as RUVBL1-interacting proteins, in addition to RUVBL2 and various known RUVBL1-interacting proteins (Fig. 1C and table S1). We confirmed these interactions by coimmunoprecipitation of SMG-10 and RPB5, and affinity purification of SBP-tagged SMG-10 (fig. S1, A to C). These results indicate that SMG-10 and RPB5 associate with the RUVBL1/2 complex. Consistent

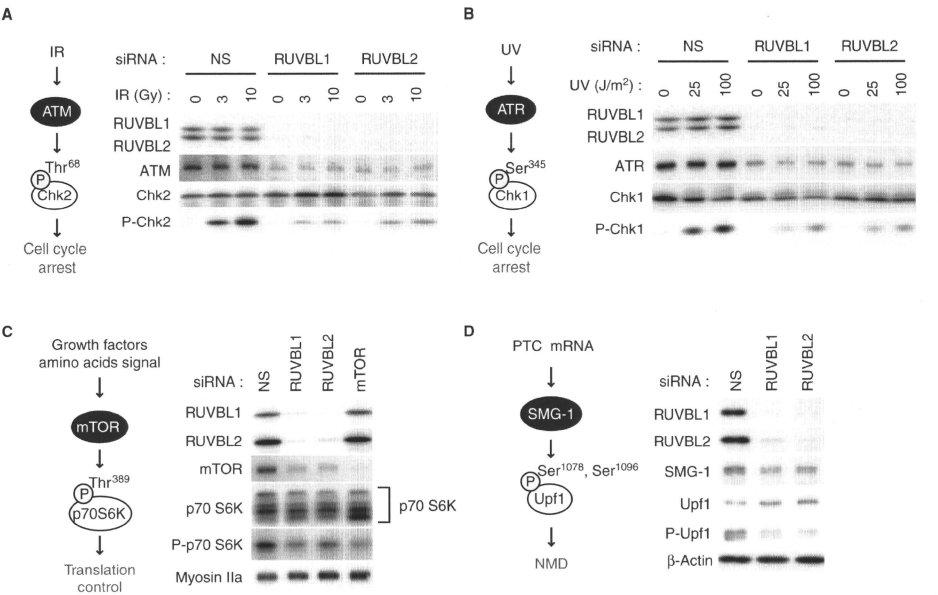

Fig. 2. Knockdown of RUVBL1 or RUVBL2 impairs PIKK signaling. (**A**) Analysis of ATM activity in HCT116 cells transfected with the indicated siRNAs and then 60 hours later unexposed or exposed to 3 or 10 Gy irradiation (IR). After 1 hour of incubation, total cell lysates were analyzed by Western blotting with the indicated antibodies. (**B**) Analysis of ATR activity in HeLa TetOff cells transfected with the indicated siRNAs and then 60 hours later unexposed or exposed to 25 or 100 J/m^2 of UV radiation. After 1 hour of incubation, total cell lysates were analyzed by Western blotting with the indicated antibodies. (**C**) Analysis of mTOR activity in HeLa TetOff cells transfected with indicated siRNAs. Sixty hours later, total cell lysates were analyzed by Western blotting with the indicated antibodies. Cells were cultured in the presence of serum, but no additional stimulation. (**D**) Analysis of SMG-1 activity in HeLa TetOff cells following the same procedures as in (C). The antibody against P-Upf1 specifically recognizes phosphorylated Upf1 residues Ser^{1078} and Ser^{1096}. All experiments were performed three times, and typical results are shown.

with these results, RUVBL1, RUVBL2, and SMG-10 interact with the N-terminal half region of SMG-1 (fig. S1D). The specificity of the interactions identified with SBP-tagged proteins was confirmed by showing that RUVBL1, RUVBL2, α-tubulin, Hsp70, SMG-10, and RPB5 failed to interact with SBP–glutathione *S*-transferase (GST) (fig. S1E).

The purified SBP-tagged RUVBL1 and SBP–SMG-10 complexes contained slowly migrating bands (Fig. 1C and fig. S1C; asterisk). Mass spectrometry analysis revealed that they contained two PIKK proteins, DNA-PKcs and TRRAP. Western blot analysis of the purified SBP-RUVBL1 complex confirmed this and further revealed the interactions between RUVBL1 and all PIKKs (DNA-PKcs, ATM, ATR, mTOR, and TRRAP) in addition to SMG-1 (Fig. 1D). Kinases in other families, such as PI3K p110α, γ, Akt, c-Jun N-terminal kinase 1 (JNK1), and extracellular signal–regulated kinases 1 and 2 (ERK1/2), were not detected in the purified SBP-RUVBL1 complexes (Fig. 1D). Thus, the RUVBL1/2 complex, and most likely SMG-10 and RPB5, can specifically associate with any kinase of the PIKK family.

RUVBL1 and RUVBL2 regulate the abundance of PIKKs and their downstream signals

The association of the RUVBL1/2 complex with all PIKKs suggested that they are involved in PIKK functions. Therefore, we investigated the effect of knockdown of RUVBL1 or RUVBL2 on downstream signals mediated by each PIKK (*4*, *5*, *9*, *12*). Knockdown of either RUVBL1 or RUVBL2 caused a significant reduction of the other protein amount, which is consistent with previous observation and the formation of these two proteins into a hexameric complex (Fig. 2) (*22*). Knockdown of RUVBL1 or RUVBL2 decreased phosphorylation of direct downstream effectors of ATM, ATR, mTOR, and SMG-1. Knockdown of either RUVBL1 or RUVBL2 decreased the phosphorylation of Chk2 at residue Thr^{68} by ATM in response to ionizing radiation (IR) (Fig. 2A), phosphorylation of Chk1 at residue Ser^{345} by ATR in response to ultraviolet (UV) radiation (Fig. 2B), phosphorylation of p70 S6K at residue Thr^{389} by mTOR (Fig. 2C), and SMG-1–mediated phosphorylation of Upf1 at residues Ser^{1078} and Ser^{1096} (Fig. 2D).

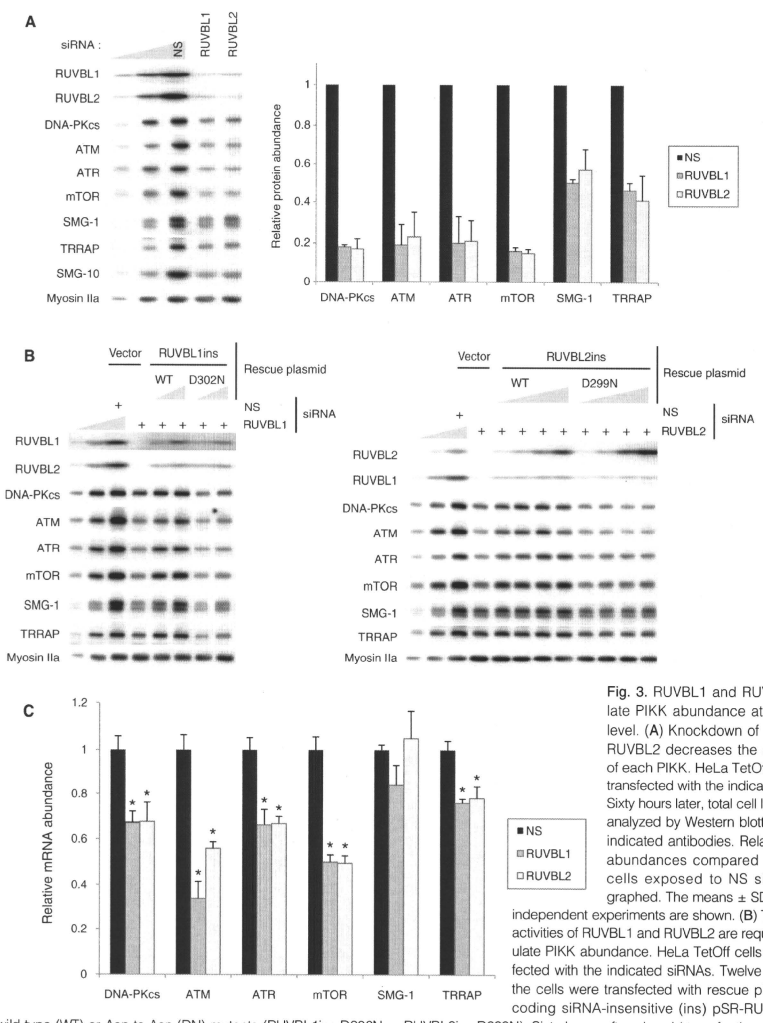

Fig. 3. RUVBL1 and RUVBL2 regulate PIKK abundance at the mRNA level. (**A**) Knockdown of RUVBL1 or RUVBL2 decreases the abundance of each PIKK. HeLa TetOff cells were transfected with the indicated siRNAs. Sixty hours later, total cell lysates were analyzed by Western blotting with the indicated antibodies. Relative protein abundances compared to those in cells exposed to NS siRNA were graphed. The means ± SD from three independent experiments are shown. (**B**) The ATPase activities of RUVBL1 and RUVBL2 are required to regulate PIKK abundance. HeLa TetOff cells were transfected with the indicated siRNAs. Twelve hours later, the cells were transfected with rescue plasmids encoding siRNA-insensitive (ins) pSR-RUVBL1ins or RUVBL2ins wild-type (WT) or Asp-to-Asn (DN) mutants (RUVBL1ins-D302N or RUVBL2ins-D299N). Sixty hours after plasmid transfections, cells were harvested and total cell lysates were analyzed by Western blotting with the indicated antibodies. To estimate the PIKK abundance, 100, 33, and 11% of NS control samples were loaded in (A) and (B). (**C**) RUVBL1 and RUVBL2 affect the amount of mRNAs that encode PIKKs. HeLa TetOff cells were transfected with the indicated siRNAs. Sixty hours later, total cytoplasmic RNAs were analyzed by real-time quantitative PCR with Taqman specific probes. Relative mRNA expression was normalized to those of GAPDH and 18*S* rRNA, and the means ± SE ($n = 3$) from three independent experiments were graphed (*$P < 0.05$ compared to NS control). All experiments were performed three times, and typical results are shown.

In addition to decreased PIKK activity, we also found that knockdown of RUVBL1 or RUVBL2 decreased the abundance of PIKKs (Fig. 2) but not the abundance of other kinases, PI3K p110α, γ, Akt, JNK1, and ERK1/2 (fig. S2, A and B). The effect on the abundance of each PIKK differed: DNA-PKcs, ATM, ATR, and mTOR were reduced to less than 25% of the amounts in cells treated with the nonsilencing (NS) small interfering RNAs (siRNAs), whereas TRRAP and SMG-1 were only reduced to 40 to 50% (Fig. 3A) of their abundance in control cells. To determine how RUVBL1 and RUVBL2 regulate the abundance of PIKKs, we tested whether protein stability, translation, or transcription was affected by knockdown of RUVBL1 and RUVBL2. Treatment of cells with cycloheximide, a protein synthesis inhibitor, failed to alter the abundance of the PIKKs in cells in which RUVBL1 and RUVBL2 were knocked down (fig. S3A). None of the proteolysis inhibitors examined restored the abundance of PIKKs in RUVBL1 and RUVBL2 knockdown cells to the abundance in cells exposed to NS siRNA (fig. S3B). However, treatment of cells with 17-AAG, an inhibitor of Hsp90, reduced the abundance of all analyzed PIKKs (fig. S3C). Hsp90 is essential for the proper protein folding and the stability of many protein kinases (*29*). Because Hsp90 associated with SMG-1 and RUVBL1 (Fig. 1, A and C) and inhibition of Hsp90 activity reduced PIKK abundance, Hsp90 may be involved in the control of PIKK abundance by the RUVBL1/2 complex. Neither SMG-10 knockdown nor RPB5 knockdown notably altered PIKK abundance or the abundance of RUVBL1 or RUVBL2 (fig. S4).

To determine if the ATPase activity of RUVBL1 and RUVBL2 was essential for controlling the abundance of PIKKs, we performed rescue experiments using siRNA-resistant RUVBL wild-type or ATPase activity–deficient mutants (DN mutants: RUVBL1 D302N or RUVBL2 D299N) (*30*). Wild-type RUVBL1 or RUVBL2 rescued the reduced PIKK abundance, whereas the DN mutants failed (Fig. 3B). These results indicate that the ATPase activities of both RUVBL1 and RUVBL2 are required to control the abundance of PIKKs; however, the exact mechanisms by which this is achieved remains unclear.

RUVBL1 and RUVBL2 associate with various transcription factors and chromatin-remodeling complexes and thereby regulate transcription (*23*). Thus, RUVBL1 and RUVBL2 may regulate the transcription of PIKK-encoding genes. Real-time quantitative PCR analysis of mRNAs from RUVBL1 or RUVBL2 knockdown cells revealed that, with the exception of SMG-1, PIKK mRNAs were decreased (Fig. 3C). Significant decreases in transcript abundance were observed in the RUVBL1 and RUVBL2 knockdown cells for mRNAs encoding DNA-PKcs, ATM, ATR, and mTOR, with ATM transcripts reduced the most. TRRAP mRNA was slightly, but significantly reduced; whereas SMG-1 mRNA was not reduced. Knockdown of RUVBL1 or RUVBL2 did not reduce the abundance of the mRNA encoding PI3K p110α (fig. S2C).

RUVBL1 and RUVBL2 affect the function of SMG-1 to contribute to nonsense-mediated mRNA decay in mammalian cells

The interactions between the RUVBL1/2 complex and each PIKK suggested that the RUVBL1/2 complex may directly regulate PIKK functions. To evaluate this possibility, we focused on SMG-1 because the knockdown effect of RUVBL1 or RUVBL2 for SMG-1 abundance was not significant and we could monitor SMG-1 function at a time point when the abundance of SMG-1 was not affected by RUVBL1 or RUVBL2 knockdown (fig. S2A). SMG-1–mediated Upf1 phosphorylation was substantially reduced by RUVBL1 or RUVBL2 knockdown (Fig. 4A). Rescue experiments with siRNA-resistant RUVBL1 wild-type or the DN mutant (RUVBL1 D302N) revealed that the ATPase activity of RUVBL1 is required for SMG-1–mediated Upf1 phosphorylation (Fig. 4B). The DN mutant had a dominant-negative effect on Upf1 phosphorylation, providing additional evidence for the involvement of these ATPases in SMG-1–mediated Upf1 phosphorylation (Fig. 4B). Thus, the RUVBL1/2 complex regulates SMG-1–mediated Upf1 phosphorylation under conditions in which SMG-1 abundance is not changed.

To show that RUVBL1 and RUVBL2 are involved in NMD, RUVBL1 or RUVBL2 was knocked down in HeLa TetOff cells transfected with either a wild-type or a PTC-containing β-globin reporter (Fig. 4C), and the half-life of the β-globin reporter mRNA (after addition of doxycycline to repress transcription of the reporter gene) was evaluated by Northern blotting. Note that the cells were harvested at time points when the knockdown of RUVBL1 or RUVBL2 did not affect the abundance of SMG-1 (36 to 44 hours after siRNA transfections) (fig. S2D). Knockdown of either RUVBL1 or RUVBL2 stabilized the PTC-containing β-globin mRNAs (Fig. 4D). In contrast, neither knockdown affected the half-life of the wild-type β-globin reporter (Fig. 4E). The requirement of RUVBL1 for NMD was also confirmed by monitoring the effect of RUVBL1 knockdown on the abundance of UHG and GAS5 mRNAs (fig. S5), which are endogenous targets of NMD (*11*, *31*). These results indicate that the RUVBL1/2 complex is required for NMD through a mechanism independent of the control of SMG-1 abundance. Because we identified SMG-10 and RPB5 as common interacting proteins of SMG-1 and RUVBL1, we also examined the effects of knockdown of SMG-10 or RPB5 on SMG-1–mediated Upf1 phosphorylation and NMD. RPB5 knockdown decreased SMG-1–mediated Upf1 phosphorylation and prolonged the half-life of PTC-containing mRNAs, suggesting that RPB5 is likely involved in NMD (fig. S6). However, knockdown of RPB5 also decreased UHG and GAS5 mRNA most likely through general transcription suppression (fig. S5). The requirement of RPB5 for NMD might provide an additional link between transcription and transcribed mRNA fate like that of other RNA polymerase II subunits (*32*). In contrast, SMG-10 knockdown did not significantly affect either Upf1 phosphorylation or NMD (Fig. 4D and figs. S5 and S6A).

The function of RUVBL1 and RUVBL2 in nonsense-mediated mRNA decay is evolutionarily conserved

To investigate whether the function of RUVBL1 and RUVBL2 in NMD is evolutionarily conserved, we tested whether the *C. elegans* orthologs of RUVBL1 and RUVBL2 (encoded by *ruvb-1* and *ruvb-2*, respectively) are involved in *C. elegans* NMD. *C. elegans* RUVB-1 and RUVB-2 are 56 and 57% identical, respectively, to human RUVBL1 and RUVBL2. We performed RNA interference (RNAi) experiments targeting *ruvb-1* and *ruvb-2* and assessed *C. elegans* NMD with two different assays. The first assay measures phenotypic suppression of *unc-54(r293)*, an allele that causes a motility phenotype that reflects the efficiency of NMD. The second assay measures directly the effects of *ruvb-1(RNAi)* and *ruvb-2(RNAi)* on the abundance of an endogenous NMD substrate.

unc-54 encodes a muscle myosin heavy chain, and *unc-54* loss-of-function mutants are strongly paralyzed. Whereas the phenotype of most *unc-54* alleles is unaffected by NMD, the motility defects of *unc-54(r293)* are suppressed by mutations that reduce or eliminate NMD (*33*, *34*). To increase the sensitivity of this phenotypic assay, we introduced mutations of two other genes into an *unc-54(r293)* genetic background. *rrf-3(pk1426)* enhances the efficiency of RNAi in *C. elegans* (*35*). *smg-1(cc546ts)* increases our ability to detect weak NMD defects. *smg-1(cc546ts)* is a temperature-sensitive allele of *smg-1*. *smg-1(cc546ts)* animals are defective for NMD at 25°C, but they are competent for NMD at 20°C. *smg-1(cc546ts) unc-54(r293)* animals exhibit normal motility at 25°C due to phenotypic suppression of *unc-54(r293)* paralysis by *smg-1(cc546ts)*, which is inactive at 25°C. They are paralyzed at 20°C as a result of NMD-dependent instability of *unc-54(r293)* mRNA [*smg-1(cc546ts)* is